LETTER

doi:10.1038/nature23475

Metabolic control of T_H17 and induced T_{reg} cell balance by an epigenetic mechanism

Tao Xu[1]*, Kelly M. Stewart[2]*, Xiaohu Wang[3]*, Kai Liu[1], Min Xie[1], Jae Kyu Ryu[1], Ke Li[1], Tianhua Ma[1,4], Haixia Wang[1], Lu Ni[3], Saiyong Zhu[1], Nan Cao[1], Dongwei Zhu[2], Yu Zhang[1], Katerina Akassoglou[1,5], Chen Dong[3]§, Edward M. Driggers[2]†§ & Sheng Ding[1,4]§

Metabolism has been shown to integrate with epigenetics and transcription to modulate cell fate and function[1–3]. Beyond meeting the bioenergetic and biosynthetic demands of T-cell differentiation[4–8], whether metabolism might control T-cell fate by an epigenetic mechanism is unclear. Here, through the discovery and mechanistic characterization of a small molecule, (aminooxy)acetic acid, that reprograms the differentiation of T helper 17 (T_H17) cells towards induced regulatory T (iT_{reg}) cells, we show that increased transamination, mainly catalysed by GOT1, leads to increased levels of 2-hydroxyglutarate in differentiating T_H17 cells. The accumulation of 2-hydroxyglutarate resulted in hypermethylation of the *Foxp3* gene locus and inhibited *Foxp3* transcription, which is essential for fate determination towards T_H17 cells. Inhibition of the conversion of glutamate to α-ketoglutaric acid prevented the production of 2-hydroxyglutarate, reduced methylation of the *Foxp3* gene locus, and increased *Foxp3* expression. This consequently blocked the differentiation of T_H17 cells by antagonizing the function of transcription factor RORγt and promoted polarization into iT_{reg} cells. Selective inhibition of GOT1 with (aminooxy)acetic acid ameliorated experimental autoimmune encephalomyelitis in a therapeutic mouse model by regulating the balance between T_H17 and iT_{reg} cells. Targeting a glutamate-dependent metabolic pathway thus represents a new strategy for developing therapeutic agents against T_H17-mediated autoimmune diseases.

To identify small molecules that reprogram T_H17 differentiation towards iT_{reg} cell fate, we screened 10,000 small molecules using $CD4^+$ naive T cells from IL-17F–RFP/FOXP3–GFP mice cultured under optimal T_H17 differentiation conditions[9] (Extended Data Fig. 1a). A small molecule, (aminooxy)acetic acid (AOA), was found to reprogram T_H17 induction to iT_{reg} cells in a dose-dependent manner (Fig. 1a and Extended Data Fig. 1b). Notably, treatment with AOA increased the phosphorylation of AMPKα in T_H17 cells, characteristic of T_{reg} cells, without affecting mechanistic target of rapamycin (mTOR) activity and c-Myc expression (Extended Data Fig. 1c). In addition, AOA-treated T_H17 cells had a similar slow proliferation rate to iT_{reg} cells (Extended Data Fig. 1d); however, the effect of AOA on cell proliferation did not impair cell survival or the ability of these T cells to differentiate into iT_{reg} cells under T_H17 cell differentiation conditions (Fig. 1a, b and Extended Data Fig. 1b, f). Notably, AOA dose-dependently promoted the induction of iT_{reg} cells, even under iT_{reg} cell culture conditions (Fig. 1c and Extended Data Fig. 1e), suggesting that AOA may directly regulate FOXP3 expression and the iT_{reg} cell program. Furthermore, AOA selectively reduced the mRNA levels of *Il17a* and *Il17f*, but not *Rorc*, in T_H17 cells and promoted the transcription of *Foxp3* in T_H17 and iT_{reg} cells (Fig. 1b, d).

AOA inhibits pyridoxal-5′-phosphate-dependent transaminases, which mediate the interconversion of α-amino and α-keto acids in a reductive amination, in which the redox balance of the reaction is maintained by concomitant conversion of glutamate (nitrogen donor) into α-ketoglutaric acid (α-KG)[10,11]. Thus, the pyridoxal-5′-phosphate/glutamate-dependent transaminase(s) involved in T-cell differentiation can be deduced by measuring stable isotopic label accumulation into various amino acids for differentiating T_H17 cells or iT_{reg} cells fed with [^{15}N]α-glutamine (Extended Data Fig. 2a). To identify the major target of AOA in T-cell differentiation, and determine whether T_H17 and iT_{reg} cells undergo active yet lineage-distinct transamination processes, T cells differentiated under T_H17 or iT_{reg} cell culture conditions were cultured with medium containing 2 mM [^{15}N]α-glutamine for 4 h, and free intracellular [^{15}N]amino acids were analysed by liquid chromatography–mass spectrometry (LC–MS). Notably, the concentration of [^{15}N]α-aspartate is 10-fold higher in differentiating T_H17 cells and iT_{reg} cells than the concentration of other detectable [^{15}N]amino acids (Fig. 1e). Moreover, approximately 50% of the cellular aspartate pool was labelled with ^{15}N, in contrast to the relatively low fractional labelling for a few other amino acids (Extended Data Fig. 2). In addition, AOA treatment reduced the total intracellular concentration of [^{15}N]α-aspartate by 90% and 75% in differentiating T_H17 cells and iT_{reg} cells, respectively (Fig. 1e). These data suggest that a primary fate of the amino group of glutamate in differentiating T_H17 cells and iT_{reg} cells was for biosynthesis of aspartic acid catalysed by glutamate oxaloacetate transaminase 1 and 2 (GOT1 and GOT2), and also that GOT1 and GOT2 serve as the major transaminases catalysing the conversion of glutamate into α-KG in these cells. Consistently, GOT1 was the only transaminase highly and differentially expressed in T_H17 and iT_{reg} cells (Fig. 1f), further suggesting an important mechanistic link for GOT1 activity in the fate determination of T_H17 cell differentiation. Short hairpin RNA (shRNA) knockdown of GOT1 in differentiating T_H17 cells inhibited T_H17 cell differentiation and reciprocally increased iT_{reg} cell differentiation (Fig. 1g, h). The effect of *Got1* shRNA could not be further increased by AOA (Extended Data Fig. 2d), also confirming the suggestion that GOT1 is the main target of AOA during T_H17 cell differentiation.

To explore how GOT1-dependent transamination regulates T_H17 cell differentiation, we profiled intracellular metabolite levels after AOA treatment by LC–MS metabolomics in differentiating T_H17 and iT_{reg} cells (day 2.5). Differentiating T_H17 cells showed a slight increase in several tricarboxylic acid (TCA) cycle intermediates, such as α-KG, succinate, fumarate, malate and citrate, compared with differentiating iT_{reg} cells, and their abundance was partially reduced by AOA in both differentiating conditions (Fig. 2a and Extended Data Fig. 3). Notably, among all of the metabolites detected, 2-hydroxyglutarate (2-HG), which is the direct product of error-prone dehydrogenase activity on the α-KG substrate, exhibits the most significantly increased level in T_H17 cells relative to iT_{reg} cells (Fig. 2a). Differentiating T_H17 cells maintained

[1]The J. David Gladstone Institutes, 1650 Owens Street, San Francisco, California 94158, USA. [2]Agios Pharmaceuticals, 38 Sidney Street, Cambridge, Massachusetts 02139, USA. [3]Institute for Immunology and School of Medicine, Tsinghua University, Beijing 100084, China. [4]School of Pharmaceutical Sciences, Tsinghua University, Beijing 100084, China. [5]Department of Neurology, University of California, San Francisco, San Francisco, California 94143, USA. †Present address: General Metabolics, LLC, 3 Huntington Road, Arlington, Massachusetts 02474, USA.
*These authors contributed equally to this work.
§These authors jointly supervised this work.

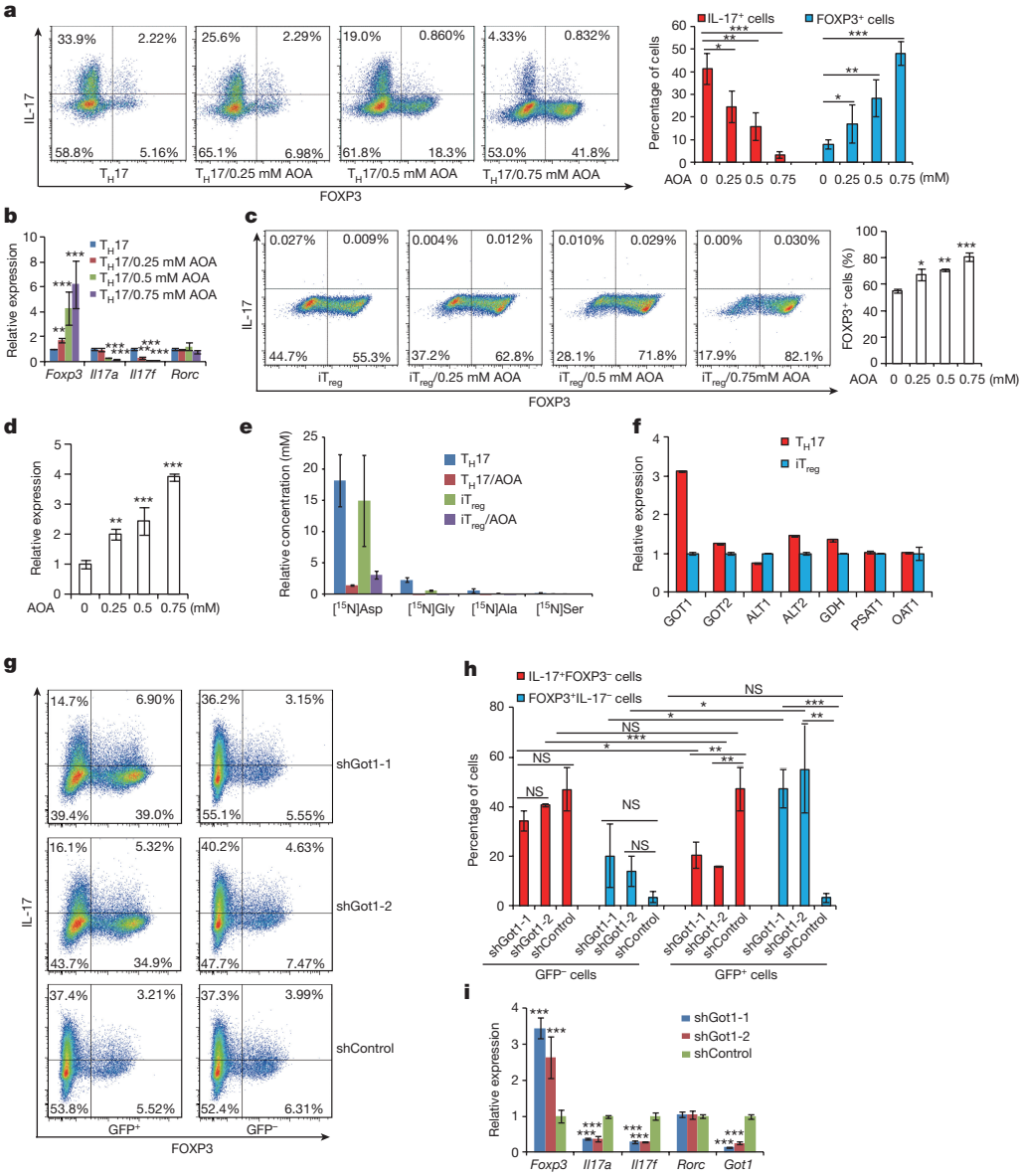

Figure 1 | AOA reprograms T_H17 cell differentiation towards iT_{reg} cells by inhibiting GOT1. a, AOA reprograms T_H17 cell differentiation towards FOXP3$^+$ iT_{reg} cells. **b**, mRNA expression in cells from **a**. **c**, AOA promotes iT_{reg} cell induction under iT_{reg} cell conditions. **d**, *Foxp3* mRNA expression from cells in **c**. **e**, GOT1 and GOT2 are the major transaminases catalysing glutamate flux into α-KG. Data are mean ± s.d. of three replicates from a representative experiment. **f**, GOT1 is highly upregulated under T_H17 cell conditions. **g**, shRNA knockdown of GOT1 (using shGot1-1 and shGot1-2) reduced T_H17 cell differentiation and reciprocally increased iT_{reg} cell differentiation. shControl denotes a non-targeting shRNA control. **h**, Statistics of cell populations from **g**. **i**, The effect of GOT1 knockdown on gene expression. In **a**, **c** and **g**, representative flow cytometry data from five (**a**) or three (**c** and **g**) independent experiments are shown. In **h**, **a** and **c** (right panels), data are mean ± s.d. of five (**a**, right) or three (**c**, right, and **h**) independent experiments. In **b**, **d**, **f** and **i**, data are mean ± s.d. of three replicates from a representative experiment of three independent experiments. NS, not significant. $^*P < 0.05$; $^{**}P < 0.01$; $^{***}P < 0.001$ by Student's *t*-test.

approximately 5–10-fold greater levels of 2-HG compared to iT_{reg} cells along the differentiation timeline (Fig. 2a and Extended Data Fig. 3b), with intracellular levels quantified to be approximately 0.2 mM. Indeed, AOA reduced the steady-state levels of 2-HG by 75% and 50% in differentiating T_H17 and iT_{reg} cells, respectively (Fig. 2a and Extended Data Fig. 3), suggesting that 2-HG synthesized from transamination-driven α-KG in differentiating T_H17 and iT_{reg} cells contributes significantly to the total amount of 2-HG. Notably, AOA treatment did not affect the L-lactic acid level in cells, indicating that AOA treatment did not affect glycolysis (Extended Data Fig. 3).

To confirm further that the conversion of total cellular glutamate into α-KG drives altered 2-HG levels, differentiating T_H17 and iT_{reg} cells were cultured with a uniformly ^{13}C-labelled glutamine ([U-^{13}C] glutamine) for 4 h, and then intracellular metabolites and isotopologues were analysed by LC–MS (Fig. 2b). With more than 80% of the intracellular glutamine pool labelled, the fractional labelling of [U-^{13}C]2-HG, [U-^{13}C]α-KG and TCA cycle intermediates was higher in T_H17 cells than in iT_{reg} cells (Fig. 2c), suggesting that more glutamine/glutamate carbon contributes to the TCA cycle and 2-HG synthesis in differentiating T_H17 cells than in iT_{reg} cells. Notably, newly synthesized 2-HG was more than 30-fold higher in T_H17 cells than in iT_{reg} cells, whereas newly synthesized α-KG is around 3-fold higher in T_H17 cells than in iT_{reg} cells (Fig. 2d). As expected, the *de novo* synthesis of both α-KG and 2-HG in iT_{reg} and T_H17 cells was inhibited by AOA, and this provides the metabolic confirmation for the decrease in the total pool as a function of AOA treatment (Fig. 2d).

To determine further the functional importance of metabolites downstream of glutamate and α-KG in specifying T_H17 and iT_{reg} cell

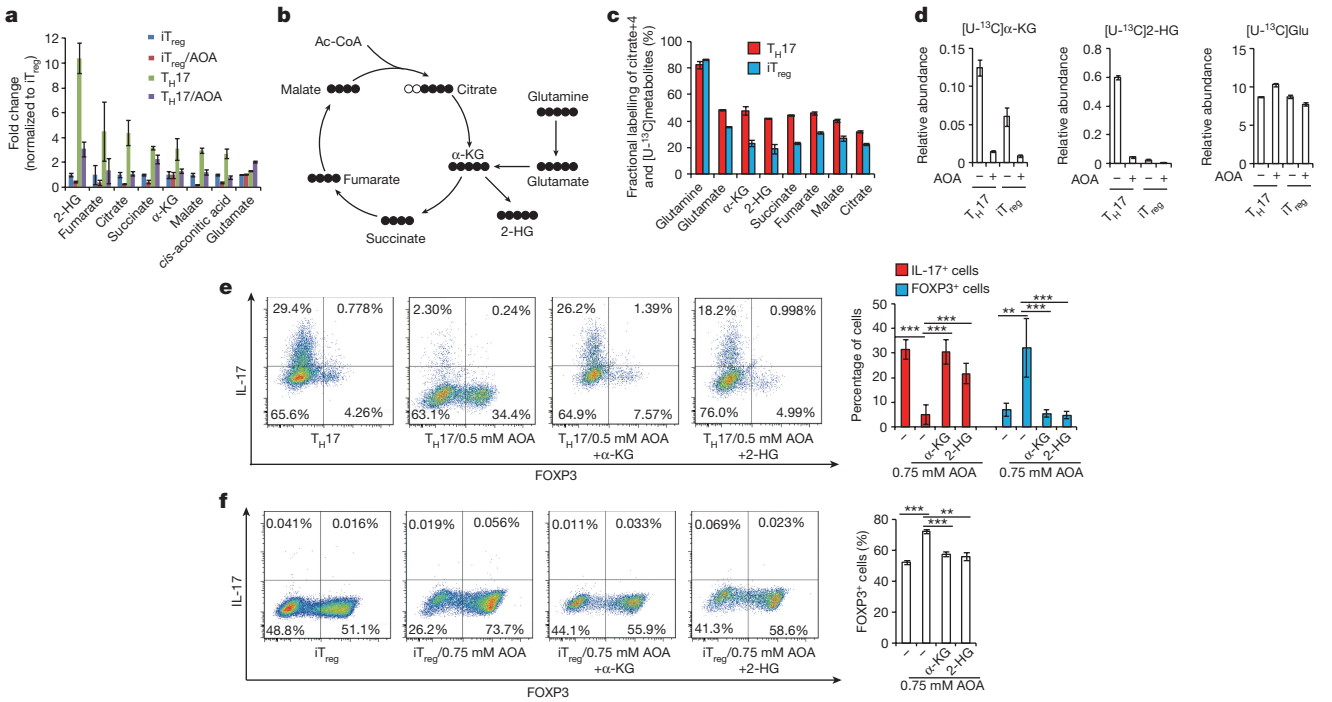

Figure 2 | 2-HG derived from glutamine and glutamate is highly increased under T_H17 cell conditions, and facilitates T_H17 cell differentiation. a, The relative abundance of significantly changing metabolites from Extended Data Fig. 3a was normalized to that in iT_{reg} cells. **b**, Schematic of labelling patterns for [U-^{13}C]glutamine feed for TCA cycle intermediates. **c**, [U-^{13}C]glutamine labelling shows that carbon of glutamine enters into TCA cycle and is responsible for 2-HG synthesis. **d**, Abundance of [U-^{13}C]2-HG ($m+5$) and [U-^{13}C]α-KG ($m+5$), normalized to intracellular [U-^{13}C]glutamine. **e**, Cell-permeable dimethyl esters of α-KG and 2-HG rescued the effects of AOA on T_H17 cell differentiation. **f**, Cell-permeable dimethyl esters of α-KG and 2-HG reversed the effect of AOA on T_H17 cell differentiation. Data are mean ± s.d. of three replicates from representative data of three (**a**) or two (**c**, **d**) independent experiments. In **e** and **f**, representative flow cytometry data from three independent experiments are shown. In the right panels of **e** and **f**, data are mean± s.d. of three independent experiments. $^{**}P < 0.01$; $^{***}P < 0.001$ by Student's *t*-test.

fate, cell-permeable α-KG, 2-HG, succinate, fumarate, malate, citrate, *N*-acetyl-cysteine (NAC) and glutathione (GSH) were individually added to AOA-containing T_H17 or iT_{reg} cell culture conditions. Among all of the metabolites examined, only cell-permeable α-KG and (*R*)-2-HG rescued the inhibitory effect of AOA on T_H17 cell differentiation or reversed its enhancing effect on iT_{reg} cell differentiation (Fig. 2e, f and Extended Data Fig. 4). Moreover, cell-permeable (*R*)-2-HG, but not α-KG (the precursor of 2-HG), directly promoted T_H17 cell differentiation (in the absence of AOA) by upregulating the expression of *Il17a* and *Il17f* and downregulating the expression of *Foxp3* in a dose-dependent manner without affecting cell survival or proliferation (Fig. 3a and Extended Data Fig. 5a, c, d), suggesting that 2-HG regulates T_H17 cell differentiation independently of cell proliferation. Similarly, cell-permeable (*R*)-2-HG, but not α-KG, inhibited *Foxp3* expression under iT_{reg} cell conditions (Fig. 3c, Extended Data Fig. 5b). A possible distinction between 2-HG and α-KG in normal T_H17 and iT_{reg} cell differentiation in the absence of AOA is that the generation of 2-HG, but not α-KG, may represent a rate-limiting step in glutamate metabolism that dictates the fate of differentiating T cells. These results showed that central carbon metabolism involving α-KG and its downstream metabolites (that is, 2-HG) is not simply a metabolomics phenomenon, but rather is a functional effector of the naive T-cell specification and its response to AOA.

2-HG has been shown to be produced by wild-type IDH1- and IDH2-mediated metabolism[12,13]. Consistently, IDH1 and IDH2 are highly expressed in differentiating T_H17 cells (Extended Data Fig. 6a, b and data not shown). Knockdown of both IDH1 and IDH2 in differentiating T_H17 cells decreased the production of 2-HG, reduced *Il17a* and *Il17f* expression, and reciprocally increased the expression of *Foxp3* (Fig. 3e, f and Extended Data Fig. 6c) without affecting *Rorc* mRNA expression or HIF1α protein expression (Extended Data Fig. 6c, f). The effect of IDH1/2 knockdown on T_H17 cell differentiation can be rescued by adding exogenous 2-HG (Extended Data Fig. 6e). The data thus suggest that α-KG and 2-HG that accumulated under T_H17 cell differentiation conditions promote further T_H17 cell differentiation.

(*R*)-2-HG suppressed *Foxp3* transcription in both T_H17 and iT_{reg} cells, and increased the transcription of *Il17a* and *Il17f*, but not *Rorc*, in differentiating T_H17 cells, indicating that (*R*)-2-HG might indirectly promote T_H17 cell differentiation by FOXP3 downregulation[14] (Fig. 3a–d). (R)-2-HG is an antagonist of TET1–TET3, which regulate FOXP3 expression redundantly by demethylating the *Foxp3* promoter and its intronic CpG island. Similar to 2-HG treatment, double knockout of *Tet1* and *Tet2* markedly increased the percentage of IL-17$^+$FOXP3$^-$ cells, and decreased the percentage of IL-17$^-$FOXP3$^+$ cells (Extended Data Fig. 7a), confirming that TET1 and TET2 also control FOXP3 expression during T_H17 cell differentiation. Consistently, 2-HG treatment promoted T_H17 cell differentiation in wild-type T cells, but the effect was largely abrogated in *Tet1* and *Tet2* double-knockout T cells (Extended Data Fig. 7a). In addition, double knockout of *Tet1* and *Tet2* partially diminished the effect of AOA on T_H17 cell differentiation (Extended Data Fig. 7b), possibly because all three TET proteins function redundantly to regulate FOXP3 expression[15,16]. These data collectively suggest that 2-HG and AOA regulate T_H17 cell differentiation at least in part by targeting TET1 and TET2. Consistently, a recent study also showed that double knockout of *Tet1* and *Tet2* in T cells resulted in unstable T_{reg} cells that were prone to conversion into T_H17 cells, and caused inflammation in several organs[15]. Notably, a reduced concentration of TGFβ (and therefore reduced recruitment of TET1 and TET2 to the *Foxp3* locus[15]) largely abrogated the promoting effect of *Tet1* and *Tet2* knockout on T_H17 cell differentiation, further confirming the role of TET1 and TET2 in FOXP3 expression during T_H17 cell differentiation (Extended Data Fig. 7c).

To further investigate the role of 2-HG and TET proteins in T_H17 cell differentiation, we examined the methylation status of the *Foxp3*

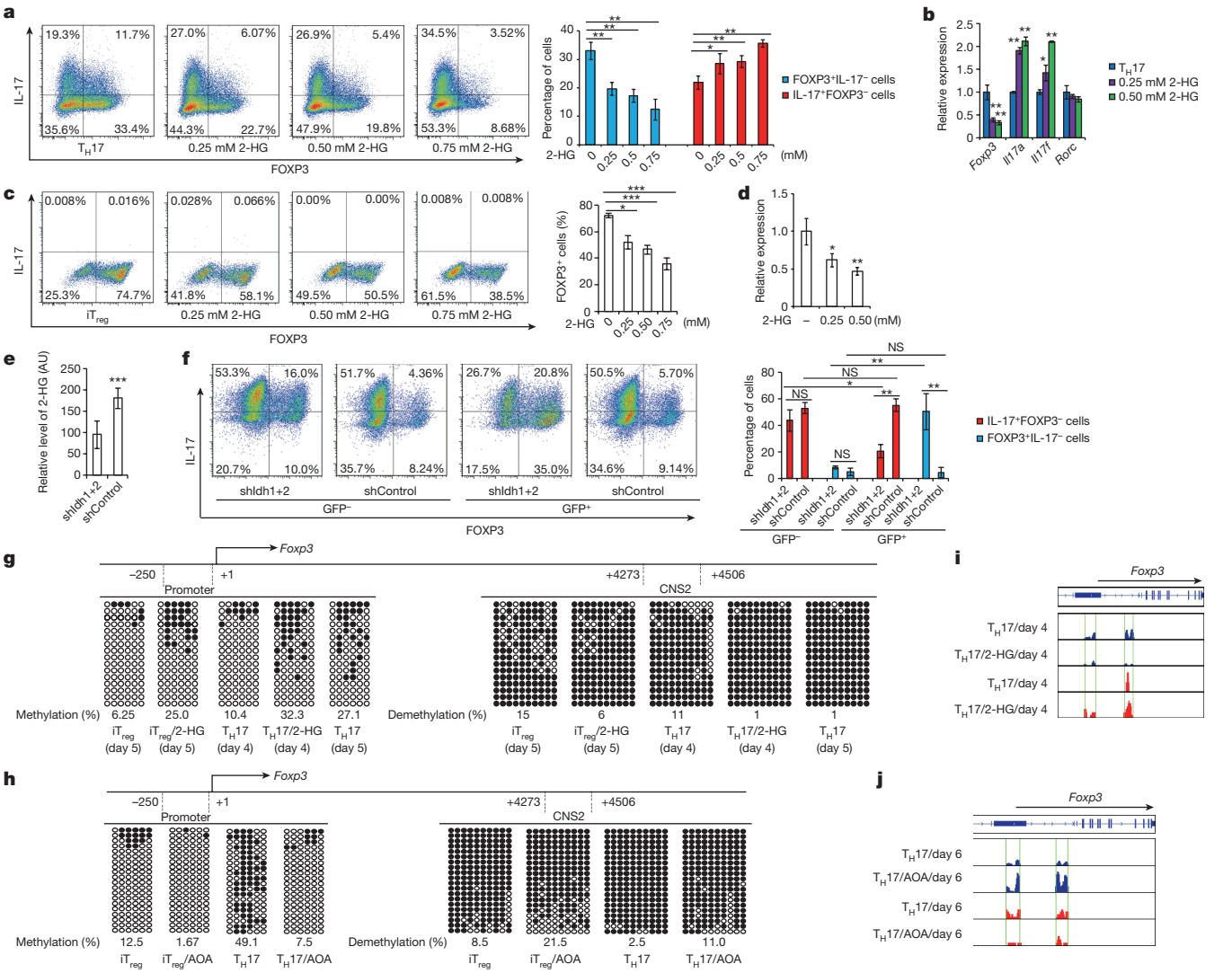

Figure 3 | 2-HG promotes T_H17 cell differentiation by promoting methylation of the *Foxp3* locus. a, Dimethyl-(*R*)-2-HG promoted T_H17 cell differentiation. **b**, mRNA expression from cells in **a**. **c**, Dimethyl-2-HG inhibited iT_{reg} cell differentiation. **d**, *Foxp3* mRNA from cells in **c**. **e**, shRNA knockdown of IDH1 and IDH2 (using shIdh1+2) decreased 2-HG production in T_H17 cell culture. **f**, Knockdown of IDH1 and IDH2 suppressed T_H17 cell differentiation and reciprocally promoted iT_{reg} cell differentiation. **g**, Exogenous dimethyl-(*R*)-2-HG promotes methylation of the *Foxp3* locus during T_H17 or iT_{reg} cell differentiation. **h**, AOA promoted hypomethylation of the *Foxp3* locus. In **g** and **h**, filled circles denote methylated cytosine, and open circles denote demethylated cytosine. **i**, **j**, The effect of 2-HG or AOA on hydroxymethylation/methylation at the *Foxp3* locus examined by (h)MeDIP–seq. 5hmC peaks (blue) or 5mC peaks (red) at the *Foxp3* locus are shown. In **g**–**j**, male mice were used owing to X-chromosome inactivation. Flow cytometry data from a representative experiment are shown in **a**, **c** and **f**. The experiments were repeated at least three times. Data in **a**, **c** and **f** (right panels) are mean ± s.d. of three independent experiments. Data in **e** ($n = 12$) are mean ± s.d. from four independent experiments. Data in **b** and **d** are mean ± s.d. of three replicates from a representative experiment of three independent experiments. $^*P < 0.05$; $^{**}P < 0.01$; $^{***}P < 0.001$ by Student's *t*-test.

promoter and CpG island by bisufite sequencing in T_H17 and iT_{reg} cells[17]. Consistent with previous studies, the *Foxp3* promoter is hypomethylated in iT_{reg} cells, and its intronic CpG island exhibits partial DNA demethylation in iT_{reg} cells[17]. Surprisingly, we found that these regions are also hypomethylated in differentiating T_H17 cells, similar to iT_{reg} cells, but are hypermethylated in fully differentiated T_H17 cells (Fig. 3g). Notably, 2-HG markedly increased the methylation levels of these regions in both differentiating T_H17 cells and iT_{reg} cells (Fig. 3g). Conversely, knockdown of IDH1 and IDH2 reduced methylation levels at the *Foxp3* promoter and conserved non-coding sequence 2 (CNS2) region (Extended Data Fig. 6d). Similarly, AOA treatment markedly decreased the methylation level at the *Foxp3* gene locus in both T_H17 and iT_{reg} cell cultures (Fig. 3h). Genome-wide distribution of 5-hydroxymethylcytosine (5hmC) and 5-methylcytosine (5mC) were then analysed by hydroxymethylated or methylated DNA immunoprecipitation followed by high-throughput sequencing (hMeDIP–seq or MeDIP-seq, respectively). In total, 330,582 peaks were enriched with 5hmC in T_H17 cells. 2-HG treatment resulted in a reduced 5hmC signal at 17,676 peaks, among which 3,402 sites also exhibited an increased 5mC signal, including the *Foxp3* locus (Fig. 3i and Extended Data Fig. 8a, b). By contrast, AOA treatment increased the 5hmC signal at 11,896 sites, among which 1,643 peaks exhibits reduced 5mC signals (Extended Data Fig. 8c, d). Consistently, AOA treatment increased the 5hmC signal at both the *Foxp3* promoter and the CNS2 region, and decreased the 5mC signal at the *Foxp3* promoter (Fig. 3j and Extended Data Fig. 8c, d) but not at the CNS2 region, probably because the changes were subtle and not detectable as the CNS2 region is always hypermethylated in iT_{reg} cells (70–80%)[17]. Notably, neither 2-HG nor AOA treatment changed the 5hmC or 5mC signal at other important lineage-specific gene loci, such as *Ifng*, *Il4*, *Il5*, *Il10*, *Il13*, *Rorc* and *Tbx21* (Extended Data Fig. 8). Notably, both AOA and 2-HG treatment affected the 5hmC and 5mC signals at

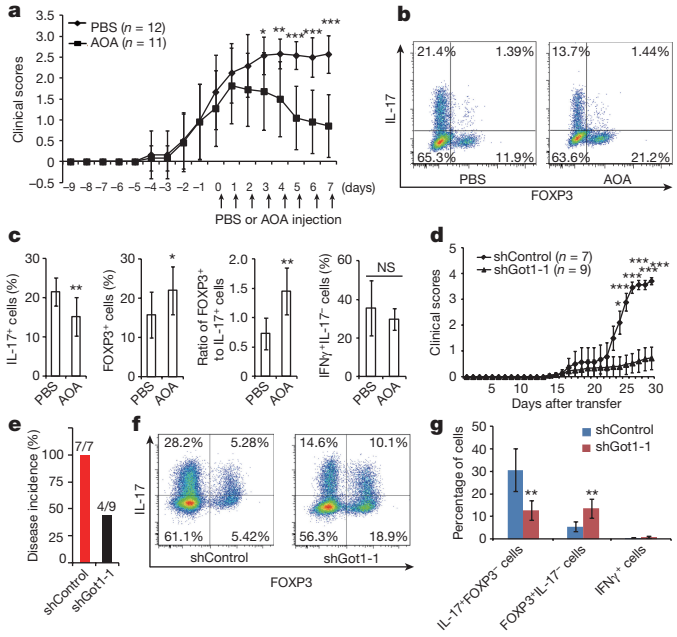

Figure 4 | AOA produced significant recovery from EAE diseases mainly by targeting *Got1*. **a**–**c**, AOA ameliorated mouse EAE diseases. **a**, Disease score. **b**, Representative flow cytometry data of T cells infiltrated into the central nervous system. **c**, Statistics of each population from **b**; $n = 11$ (control), $n = 10$ (AOA). The results in **a**–**c** are combinations of two experiments. **d**–**g**, T_H17-polarized adoptive transfer EAE showed that knockdown of *Got1* ameliorated mice EAE diseases. **d**, Disease score. **e**, Disease incidence. **f**, Representative flow cytometry data of T cells infiltrated into the central nervous system (gated on Thy1.1$^+$ cells). **g**, Statistics for the T cells infiltrated into the central nervous system. Results in **d**–**g** are from one representative experiment of two experiments. Data in **a**, **c** and **g** are mean ± s.d. Data in **d** are mean ± s.e.m. $^*P < 0.05$; $^{**}P < 0.01$; $^{***}P < 0.001$ by Student's *t*-test.

121 sites (97 genes, including non-coding RNAs), many of which are direct FOXP3 targets, such as *Foxp1* and *Bach2* (Extended Data Fig. 8e, f, Supplementary Data 2), indicating that changes in 5hmC and 5mC at these targets may be caused indirectly by FOXP3 expression. These epigenetics analyses, together with gene expression data, strongly suggest that AOA and 2-HG regulate T_H17 cell differentiation indirectly by altering the expression of *Foxp3*, but not of other T-lineage-related genes.

To examine the functional relevance of our findings, experimental autoimmune encephalomyelitis (EAE) was induced as described[18]. AOA or control vehicle was injected daily intraperitoneally after most mice had developed apparent diseases. Notably, the administration of AOA caused a significant recovery from EAE diseases in this therapeutic disease model (Fig. 4a). In addition, the total number of mononuclear cells infiltrating into the central nervous system was markedly reduced in AOA-treated mice compared to control mice (Extended Data Fig. 9d). The treatment of AOA significantly reduced the percentage of IL-17-producing T cells and increased the percentage of FOXP3$^+$ T cells ($P < 0.05$) without affecting the percentage of IFNγ^+ cells ($P > 0.05$) in the central nervous system (Fig. 4b, c). The ratio of FOXP3$^+$ cells to IL-17$^+$ cells is much higher in AOA-treated mice than in control mice (Fig. 4c). To investigate further the physiological importance of GOT1 *in vivo*, an adoptive transfer model using CD4 naive T cells from 2D2 mice (constitutively expressing MOG_{35-55} specific T-cell antigen receptors[19]) was performed. The cells undergoing T_H17 cell differentiation were infected with a virus containing *Got1* shRNA or control shRNA and Thy1.1 (CD90.1), and the infected cells were then transferred into wild-type mice. In this T_H17-polarized transfer EAE model, disease severity plus the total number of mononuclear cells infiltrating into the central nervous system were significantly reduced in mice receiving GOT1-knockdown cells compared with those receiving control-shRNA-infected cells (Fig. 4d, e, Extended Data Fig. 9a, d). The percentage of IL-17-producing T cells and FOXP3$^+$ T_{reg} cells infiltrating into the central nervous system were significantly decreased and increased, respectively by GOT1 knockdown, whereas IFNγ^+ T cells were not readily detectable (Fig. 4f, g, and Extended Data Fig. 9). Our study thus demonstrates that selectively targeting the glutamate metabolic pathway could alter the balance of T_H17 and T_{reg} cells both *in vitro* and *in vivo*, and may represent a new strategy for addressing T_H17-mediated autoimmune diseases.

In summary, we have shown that increased transamination via GOT1 leads to a much greater accumulation of 2-HG in differentiating T_H17 cells than in iT_{reg} cells, and this promoted the methylation of the *Foxp3* gene locus and silenced *Foxp3* gene expression. Notably, we found that 2-HG levels in differentiating T_H17 cells (for example, 0.1–0.4 mM) were much lower than that in human cancer cells containing *IDH1* and *IDH2* mutations (≥1 mM). Nonetheless, endogenous 2-HG accumulations under T_H17 conditions and experiments with exogenously added 2-HG in T_H17 cell culture correlate well with hypermethylation of the *Foxp3* gene locus and reduced mRNA and protein levels of FOXP3 in fully differentiated T_H17 cells, suggesting that different cell types may exhibit differential sensitivity to 2-HG levels. Manipulating a single step in a glutamate metabolic pathway could change T_H17 cell fate by affecting methylation of the *Foxp3* gene locus, and ameliorate mouse EAE disease by regulating the T_H17 and iT_{reg} cell balance, highlighting the importance of cellular metabolism in the determination of T-cell fate.

Online Content Methods, along with any additional Extended Data display items and Source Data, are available in the online version of the paper; references unique to these sections appear only in the online paper.

Received 14 May 2015; accepted 4 July 2017.
Published online 2 August 2017.

1. Wellen, K. E. & Thompson, C. B. A two-way street: reciprocal regulation of metabolism and signalling. *Nat. Rev. Mol. Cell Biol.* **13,** 270–276 (2012).
2. Lu, C. & Thompson, C. B. Metabolic regulation of epigenetics. *Cell Metab.* **16,** 9–17 (2012).
3. Kaelin, W. G. Jr & McKnight, S. L. Influence of metabolism on epigenetics and disease. *Cell* **153,** 56–69 (2013).
4. Pearce, E. L., Poffenberger, M. C., Chang, C. H. & Jones, R. G. Fueling immunity: insights into metabolism and lymphocyte function. *Science* **342,** 1242454 (2013).
5. Pearce, E. L. & Pearce, E. J. Metabolic pathways in immune cell activation and quiescence. *Immunity* **38,** 633–643 (2013).
6. Wang, R. & Green, D. R. Metabolic checkpoints in activated T cells. *Nat. Immunol.* **13,** 907–915 (2012).
7. Shi, L. Z. *et al.* HIF1α-dependent glycolytic pathway orchestrates a metabolic checkpoint for the differentiation of T_H17 and T_{reg} cells. *J. Exp. Med.* **208,** 1367–1376 (2011).
8. Berod, L. *et al. De novo* fatty acid synthesis controls the fate between regulatory T and T helper 17 cells. *Nat. Med.* **20,** 1327–1333 (2014).
9. Yang, X. O. *et al.* Molecular antagonism and plasticity of regulatory and inflammatory T cell programs. *Immunity* **29,** 44–56 (2008).
10. DeBerardinis, R. J. *et al.* Beyond aerobic glycolysis: transformed cells can engage in glutamine metabolism that exceeds the requirement for protein and nucleotide synthesis. *Proc. Natl Acad. Sci. USA* **104,** 19345–19350 (2007).
11. Son, J. *et al.* Glutamine supports pancreatic cancer growth through a KRAS-regulated metabolic pathway. *Nature* **496,** 101–105 (2013).
12. Wise, D. R. *et al.* Hypoxia promotes isocitrate dehydrogenase-dependent carboxylation of α-ketoglutarate to citrate to support cell growth and viability. *Proc. Natl Acad. Sci. USA* **108,** 19611–19616 (2011).
13. Terunuma, A. *et al.* MYC-driven accumulation of 2-hydroxyglutarate is associated with breast cancer prognosis. *J. Clin. Invest.* **124,** 398–412 (2014).
14. Zhou, L. *et al.* TGF-β-induced Foxp3 inhibits T_H17 cell differentiation by antagonizing RORγt function. *Nature* **453,** 236–240 (2008).
15. Yang, R. *et al.* Hydrogen sulfide promotes Tet1- and Tet2-mediated *Foxp3* demethylation to drive regulatory T cell differentiation and maintain immune homeostasis. *Immunity* **43,** 251–263 (2015).
16. Yue, X. *et al.* Control of Foxp3 stability through modulation of TET activity. *J. Exp. Med.* **213,** 377–397 (2016).
17. Kim, H. P. & Leonard, W. J. CREB/ATF-dependent T cell receptor-induced *FoxP3* gene expression: a role for DNA methylation. *J. Exp. Med.* **204,** 1543–1551 (2007).
18. Xu, T. *et al.* Ursolic acid suppresses interleukin-17 (IL-17) production by selectively antagonizing the function of RORγt protein. *J. Biol. Chem.* **286,** 22707–22710 (2011).

19. Bettelli, E. *et al.* Myelin oligodendrocyte glycoprotein-specific T cell receptor transgenic mice develop spontaneous autoimmune optic neuritis. *J. Exp. Med.* **197,** 1073–1081 (2003).

Supplementary Information is available in the online version of the paper.

Acknowledgements S.D. is supported by funding from the Gladstone Institutes and Tsinghua University. X.W. is supported by a grant from NFSC (31570884). A Race to Erase MS Young Investigator Award, and American Heart Association Scientist Development Grant were awarded to J.K.R. and NIH/NINDS R35 NS097976 was awarded to K.A. We thank G. Howard for help with editing the manuscript, and H. W. Lim for discussion.

Author Contributions T.X. and S.D. conceived the project; T.X., K.M.S., X.W., C.D., E.M.D. and S.D. designed the experiments. T.X., K. Li, T.M., H.W., S.Z., N.C. and Y.Z. performed the *in vitro* experiments; T.X. prepared the samples for metabolic analysis; K.M.S. conducted all metabolomics and flux analysis; D.Z. helped to analyse 2-HG levels. X.W. and L.N. performed active EAE experiments; T.X. and J.K.R. performed transfer EAE experiment (T.X. prepared cells and injected cells into mice, and J.K.R. scored the mice, and T.X. and J.K.R. analysed T cells infiltrated into the central nervous system). M.X. prepared chemicals. K. Liu analysed the data from (h)MeDIP–seq. K.A. designed experiments and analysed data. T.X., K.M.S., X.W., C.D., E.M.D. and S.D. wrote the manuscript; K.A., C.D., E.M.D. and S.D. edited the manuscript. All authors read and approved the final manuscript.

Author Information Reprints and permissions information is available at www.nature.com/reprints. The authors declare no competing financial interests. Readers are welcome to comment on the online version of the paper. Publisher's note: Springer Nature remains neutral with regard to jurisdictional claims in published maps and institutional affiliations. Correspondence and requests for materials should be addressed to C.D. (chendong@tsinghua.edu.cn), E.M.D. (edward.driggers@generalmetabolics.com) or S.D. (sheng.ding@gladstone.ucsf.edu).

Reviewer Information *Nature* thanks L. O'Neill and the other anonymous reviewer(s) for their contribution to the peer review of this work.

METHODS

Reagents and cell culture. T cells were cultured in Advanced RPMI 1640 (Invitrogen, 12633) supplemented with 10% FBS (Invitrogen), penicillin–streptomycin (Invitrogen), 55 μM β-mercaptoethanol, and 2 mM glutamine.

T-cell differentiation. CD4 naive T cells ($CD4^+CD25^-CD62^{high}CD44^{low}$) were sorted from IL-17F–RFP/FOXP3–GFP mice, which were characterized previously or wide-type C57BL/6 mice (6–10-week-old male or female mice were used unless specified). Approximately 0.4 million cells were plated into 48-well-plates coated with anti-mouse CD3 (clone 145-2C11, eBioscience) (2 μg ml^{-1}) and anti-mouse CD28 (clone 37.51, eBioscience) (1 μg ml^{-1}). The differentiation conditions for T cells are as followed: 0.5 ng ml^{-1} (or indicated) TGFβ, 200 U ml^{-1} mouse IL-2, 2 μg ml^{-1} anti-IFNγ and 2 μg ml^{-1} anti-mouse IL-4 for iT_{reg}, 2.5 ng ml^{-1} TGFβ, 10 ng ml^{-1} mouse IL-1β, 10 ng ml^{-1} mouse IL-6, 10 ng ml^{-1} mouse IL-23, 2 μg ml^{-1} anti-mouse IFNγ, and anti-mouse IL-4 for T_H17. All the cytokines are from R&D systems. The cells were supplemented with new medium at day 4. For cases in which small-molecule compounds were present, fresh medium containing the same concentration of compounds was used. When necessary, the individual metabolite was added into the T-cell culture 6 h after initial cell plating. On day 6, the cells were analysed for IL-17F–RFP and FOXP3–GFP or the cells were collected and restimulated for 4–6 h with phorbol myristate acetate (PMA), ionomycin, and Golgi-stop for intracellular staining in absence of indicated compounds.

Antibodies. Anti-IDH2 was from Abcam (ab131263), anti-IDH1 was from Cell Signaling Technology (8137S), and anti-HIF1α was from Novus Biologicals (NB100-105). Anti-mouse CD3 (clone 145-2C11, 16-0031), anti-mouse CD28 (clone 37.51, 16-0281), anti-mouse IFNγ (clone XMG1.2, 16-7311), anti-mouse IL-4 (clone 11B11, 16-7041), anti-mouse FOXP3 (clone FJK-16s, 17-5773) were from eBioscience. Anti-mouse CD4 (clone RM4-5, 550954), anti-mouse CD25 (clone 7D4, 558642), anti-mouse CD44 (clone IM7, 559250), anti-mouse CD62L (clone MEL-14, 560507), anti-mouse IL-17 (clone TC11-18H10, 559502), anti-mouse IFNγ (clone XMG1.2, 561040, for staining) and anti-CD90.1 (Thy1.1) (clone OX-7, 561406) were from BD Bioscience.

mRNA expression analysis by qRT–PCR. At the end of differentiation (day 6), T cells were re-stimulated with plate-coated anti-CD3 and anti-CD28 for 5 h in the absence of any small-molecule compounds or metabolites. qRT–PCR was performed to evaluate mRNA expression of *Foxp3*, *Il17a*, *Il17f* and *Rorc*. For differentiating T_H17 or iT_{reg} cells, cells were collected on day 2.5 or at the indicated time for mRNA expression analysis. The expression was normalized to β-actin (*Actb*). All primers are listed in Supplementary Data 1.

Intracellular metabolomics/broad profiling. CD4 naive T cells, differentiating T_H17 cells (day 2.5), and iT_{reg} cells (day 2.5) were collected. A solution of 80:20 methanol:H_2O was used to extract intracellular metabolites. The extracted samples were analysed with LC–MS metabolomics. 200 ng ml^{-1} of extraction standard (L-glutamic acid-$^{13}C_5$,^{15}N-d_5) was added into samples, and the peak value for each metabolite was normalized to an extraction standard. The data were transformed into log_2 and clustered. Cell extracts obtained as described above were analysed for relative abundance of ^{13}C and ^{15}N metabolites by quadruple Fourier-transform ion cyclotron resonance-based LC–MS (Q-FTICR) using scheduled selective reaction monitoring (SRM) for each metabolite of interest, with the detector set to negative mode[20]. Quantification of intracellular 2HG was conducted as described[21].

[U-^{13}C]glutamine or [^{15}N]α-glutamine flux analysis. CD4 naive T cells, differentiating T_H17 or iT_{reg} cells (68 h) were incubated with fresh media before labelling. The cells were then cultured for 4 h at 37 °C with medium in which the glutamine was replaced with the corresponding stable isotope label: 2 mM [U-^{13}C]glutamine or 2 mM [^{15}N]α-glutamine for 4 h at 37 °C. The cells were quickly collected and quickly washed with PBS, pelleted, and snap frozen in liquid nitrogen. The frozen samples were kept in −80 °C until extraction. Cell extracts were prepared by first adding 80:20 methanol:H_2O at −60 °C to the frozen pellets and collecting the supernatant after centrifugation at 4 °C. The extracted samples were analysed by high-resolution LC–MS. Unlabelled glutamine-fed cells were used as background.

Negative mode metabolomics. Cell extracts obtained as described above were analysed for relative abundance of metabolites by LC–MS using scheduled selective reaction monitoring (SRM) for each metabolite of interest, with the detector set to negative mode[20]. Before injection, dried extracts were reconstituted in LC–MS grade water. Liquid chromatogrpahy separation was achieved by reverse-phase ion-pairing chromatography as described[22].

Amino acid profiling. The U-HPLC system consisted of a Thermo Fisher Scientific U-HPLC pumping system, coupled to an autosampler and degasser. Chromatographic separation of the intracellular metabolites was achieved by usage of a reversed phase Atlantis T3 (3 μm, 2.1 mm ID × 150mm) column (Waters) and by implementation of a gradient elution program. The elution gradient was carried out with a binary solvent system consisting of 0.1% formic acid and 0.025% heptafluorobutyric acid in water (solvent A) and in acetonitrile (solvent B) at a constant flow rate of 400 μl min^{-1}. The linear gradient employed was as follows: 0–4 min increase from 0 to 30% B, 4–6 min from 30 to 35% B, 6–6.1 min from 35 to 100% B and hold at 100% B for 5 min, followed by 5 min of re-equilibration. The column oven temperature was maintained at 25 °C and sample volumes of 10 μl were injected. HRAM data were acquired using a QExactive Orbitrap mass spectrometer (Thermo Fisher Scientific), which was equipped with a heated electrospray ionization source (HESI-II), operated in positive mode. Ionization source working parameters were optimized; the heater temperature was set to 300 °C, ion spray voltage was set to 3,500 V. An *m/z* scan range from 70 to 700 was chosen and the resolution was set at 70,000. The automatic gain control (AGC) target was set at 1×10^6 and the maximum injection time was 250 ms. Instrument control and acquisition was carried out by Xcalibur 2.2 software (Thermo Fisher Scientific).

Methylation analysis by bisulfite sequencing. The method is the same as described. In brief, genomic DNA was purified with the Blood and Cell Culture DNA Midi Kit (Qiagen). Bisufite conversion of genomic DAN was performed using EpiTect Bisulfite kit (Qiagen), according to the manufacturer's instructions. The primers used to amplify the *Foxp3* promoter and its intronic CpG island are described in the Supplementary Information. The PCR product was run on 2% agarose, purified and cloned using TOPO TA Cloning Kit with PCR4. Clones are picked for Sanger sequencing.

Retrovirus preparation and T-cell infection. shRNAs (synthesized DNA oligonucleotides) after annealing were cloned into PMKO.1-GFP retrovirus or PMKO.1-Thy1.1-mRFP vector. The plasmids and pCL-ECO (1:1) were transfected into 293T cells (ATCC, CRL-3216; all cells were tested for mycoplasma contamination) with Fugene HD4 (Promega). The medium was changed 6 h after transfection, and the cells were further cultured for 48–72 h. The supernatant was then collected and filtered using 45-μm filters. The supernatant containing the viruses was added into pre-activated CD4 T cells (20 h after initial plating). The cells were spin-infected at 1,000*g* for 2 h and cultured in an incubator for another 2 h. The cells were washed and cultured under T_H17 cell conditions for an additional 4 days. New medium was added if necessary. At day 5, the cells are collected for sorting GFP^+ and GFP^- cells. Sorted cells were further cultured until day 6, and re-stimulated for intracellular staining or mRNA analysis, as described above.

Mouse EAE model. EAE was induced by immunizing mice (12 weeks old, 5–6 C57BL/6 mice per group) twice with 300 μg of $MOG_{35–55}$ peptide (amino acids 35–55; MEVGWYRSPFSROVHLYRNGK) emulsified in complete Freund's adjuvant, followed by pertussis toxin injection and analysed as described[18]. The disease scores were assigned on a scale of 0–5 as follows: 0, none; 1, limp tail or waddling gait with tail tonicity; 2, wobbly gait; 3, hind limb paralysis; 4, hind limb and forelimb paralysis; 5, death. When the disease phenotype is very obvious (average score >1), PBS or AOA (750 μg per mouse) was intraperitoneally injected every day (mice were randomly assigned to treatment groups, and scored in a blinded manner). After 8 days of administration of AOA or PBS, the mice were anaesthetized, and cells infiltrated into brain and spinal cord were collected for analysis. For adoptive transfer EAE, CD4 naive T cells isolated from 2D2 mice (https://www.jax.org/strain/006912) were cultured under T_H17 cell conditions for 20 h, and then the cells were infected with virus containing shGot1 or control shRNA and a cell surface protein, $Thy1.1^+$ (which does not express in C57BL/6 background mice). At the end of the differentiation, the cells were purified, and 6×10^7 cells were intraperitoneally injected into wild-type C57BL/6 recipient mice (8–10-week-old female mice). The recipient mice were irradiated with sublethal X-ray (5 Gy) before cells injection. PTX (500 ng per mouse) was intraperitoneally injected later on the day of transfer and two days later. The disease was scored daily thereafter as above. Mice were randomly assigned to treatment groups, and scored in a blinded manner. Experimental groups were unblinded to treatment assignment at the end of the experiments to ensure experimenter bias was not introduced. At the end of experiment, the mice were euthanized for analysis of the T cells infiltrated into the central nervous system. Mice that did not develop symptoms of EAE were not excluded from the analysis. Power analysis was used to calculate the sample size. 4 mice per group is enough for calculation, here we used 5–6 in active EAE, or 7–9 mice in adoptive transfer EAE to get a more confident dataset. When indicated, the statistical significance was determined by Student's *t*-test (*$P < 0.05$; **$P < 0.01$; ***$P < 0.001$). All animal work was approved by the institutional IACUC committee.

Mice. Tet1tm1.1Jae/J (JAX 017358, $Tet1^{+/-}$), B6.129S-Tet2tm1.1Iaai/J (JAX 017573, $Tet2^{fl/fl}$), and Tg(Cd4-cre)1Cwi/BfluJ (JAX 017336, Cd4-Cre) mice were purchased from Jackson Laboratory. We first got $Tet1^{+/-}Tet2^{fl/fl}CD4\text{-}Cre^+$, then mated them to generate $Tet1^{-/-}Tet2^{fl/fl}CD4\text{-}Cre^+$ mice. 2D2 mice (https://www.jax.org/strain/006912) were purchased from Jax.

MeDIP–seq/hMeDIP–seq. DNA was purified from differentiating T_H17 cells (in the absence or presence of dimethyl (*R*)-2-HG), or T_H17 cells at the end of differentiation (in the absence or in presence of AOA), and sheared into 200–500-bp fragments using a Covaris S2 sonicator. DNA fragments were then end-repaired, adenylated, and adaptor added using the Nextflex ChIP–seq

preparation kit (Bio Scentific) following the manufacturer's protocol. The ligated DNA was then denatured into single-stranded DNA for chromatin immunoprecipitation (ChIP). The ChIP was done by incubating the DNA with anti-5mC or 5hmC (from Active Motif) following the manufacturer's protocol. After ChIP, the eluted DNA was PCR amplified and sequenced on Hiseq-2500.

Data analysis for (h)MeDIP–seq. Raw FASTQ Reads are trimmed using the fastq-mcf program to remove any Illumina adaptor sequence. Trimmed reads are aligned to the genome assembly of *Mus musculus* reference genome (NCBI37/mm9) using Bowtie2[1]. 5hmC and 5mC peak identification was performed with MACS[2] using non-duplicate reads from each immunoprecipitation sample and its corresponding input control sample. Parameters are as follows: effective genome size = 1.87×10^9; band width = 200; ranges for calculating regional lambda are: peak_region, 1,000, 5,000, 10,000; and Benjamini–Hochberg q-value cutoff = 0.01 to identify confident peaks. Read counts of all peak regions were extracted from each samples by bedtools multicov[3] and used for further analysis of quantitative changes. Peak regions with a greater than 30 read count in all 5hmC sample or 10 in 5mC samples are kept. Each region for each sample is scored by the read count in this region normalized to the total number of mapped reads in each sample. The difference is computed as peak region intensity between samples as $\log_2$ fold change. Peak region annotation is performed with Homer tools suite to identify genomic features and associated genes based on distance to the nearest transcription start site. Peak region intensities of larger than 2-fold difference for 5hmC or 1.8-fold for 5mC were highlighted by scatter plot. Normalized pileup files are converted to bigwig (http://genome.ucsc.edu/goldenpath/help/bigWig.html) for visualization in IGV[26–28].

Data availability. The NCBI SRC accession number for the MeDIP–seq and hMeDIP–seq experiments reported in this manuscript is BioProject PRJNA360149.

20. Munger, J. *et al.* Systems-level metabolic flux profiling identifies fatty acid synthesis as a target for antiviral therapy. *Nat. Biotechnol.* **26,** 1179–1186 (2008).
21. Kernytsky, A. *et al.* IDH2 mutation-induced histone and DNA hypermethylation is progressively reversed by small-molecule inhibition. *Blood* **125,** 296–303 (2015).
22. Buescher, J. M., Moco, S., Sauer, U. & Zamboni, N. Ultrahigh performance liquid chromatography–tandem mass spectrometry method for fast and robust quantification of anionic and aromatic metabolites. *Anal. Chem.* **82,** 4403–4412 (2010).
23. Ichiyama, K. *et al.* The methylcytosine dioxygenase Tet2 promotes DNA demethylation and activation of cytokine gene expression in T cells. *Immunity* **42,** 613–626 (2015).
24. Toker, A. *et al.* Active demethylation of the Foxp3 locus leads to the generation of stable regulatory T cells within the thymus. *J. Immunol.* **190,** 3180–3188 (2013).
25. Zheng, Y. *et al.* Genome-wide analysis of Foxp3 target genes in developing and mature regulatory T cells. *Nature* **445,** 936–940 (2007).
26. Zhang, Y. Model-based analysis of ChIP–seq (MACS). *Genome Biol.* **9,** R137 (2008).
27. Langmead, B., Trapnell, C., Pop, M. & Salzberg, S. L. Ultrafast and memory-efficient alignment of short DNA sequences to the human genome. *Genome Biol.* **10,** R25 (2009).
28. Quinlan, A. R. & Hall, I. M. BEDTools: a flexible suite of utilities for comparing genomic features. *Bioinformatics* **26,** 841–842 (2010).

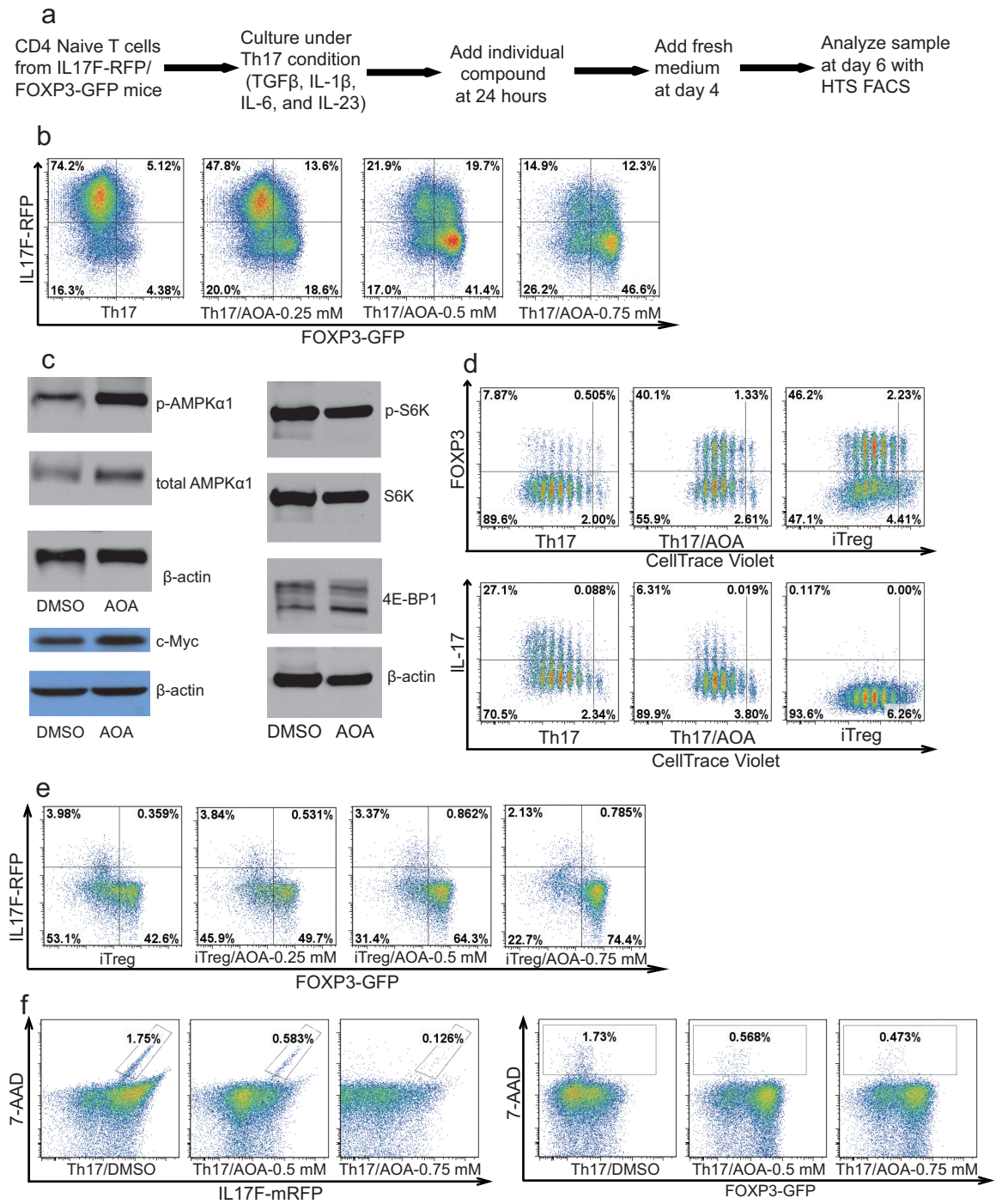

Extended Data Figure 1 | AOA reprograms T_H17 cell differentiation towards iT_{reg} cells. a, Schematic of the screening procedure. **b**, Effects of AOA on T_H17 cell differentiation. **c**, The effect of AOA on mTOR, AMPK and c-Myc. Differentiating T_H17 cells (with or without 0.75 mM AOA) were collected for analysis of phosphorylated AMPKα1 (p-AMPKα1), the mTOR downstream signalling proteins S6K and 4E-BP1, and c-Myc and β-actin. Dimethylsulfoxide (DMSO) was used as a control. **d**, The effect of AOA on the proliferation of T_H17 cells. CD4 naive T cells were labelled with CellTrace Violet, and then cultured under T_H17 or iT_{reg} cell conditions (which were the same as T_H17 cell conditions except without IL-1β, IL-6 and IL-23). At the end of experiment, the cells were analysed by intracellular staining. **e**, AOA promoted iT_{reg} cell differentiation. **f**, AOA did not affect the survival of T_H17 cell culture. The cells were differentiated under T_H17 cell conditions with or without AOA. At the end of the differentiation, 7-AAD was added and the cells were immediately collected for analysis.

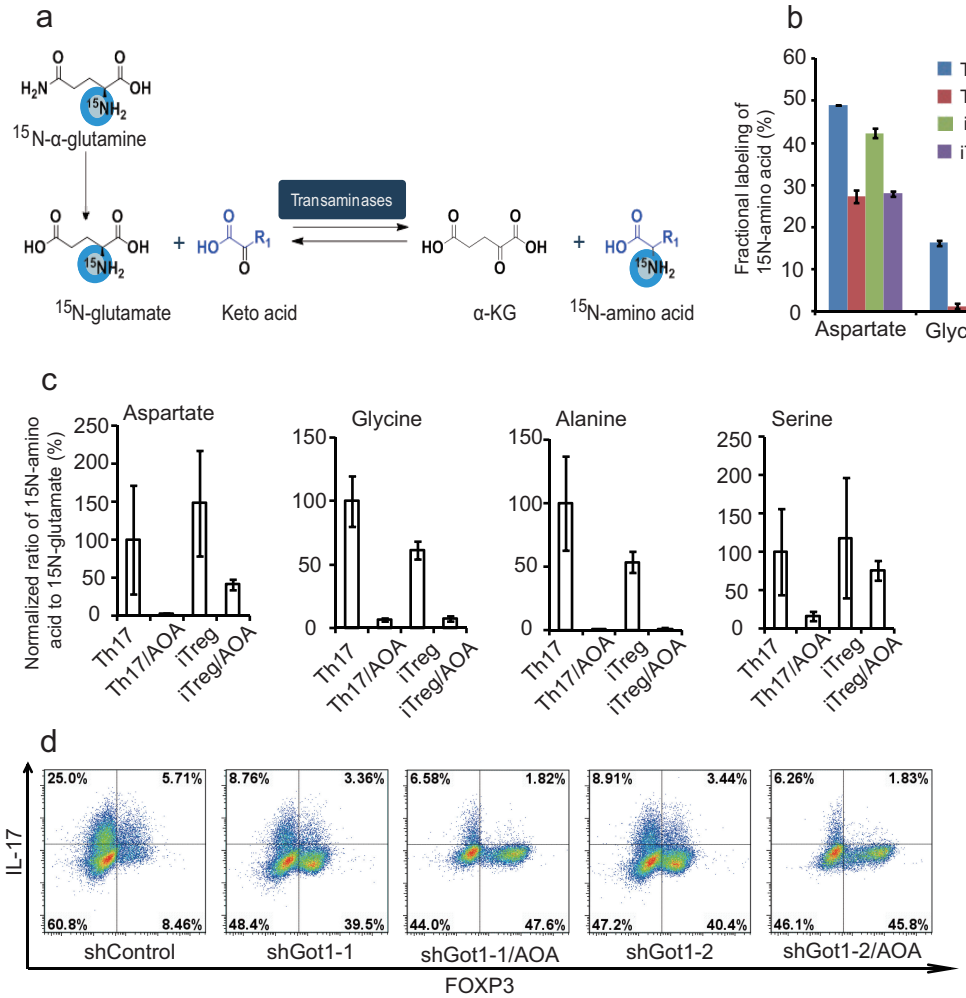

Extended Data Figure 2 | ^{15}N-labelling analysis showed that GOT1 mediates most transamination reactions and represents the main target for AOA in T_H17 cells. a, Schematic of [^{15}N]α-glutamine metabolism in the transamination reaction. **b**, The ratios of ^{15}N-labelled amino acids to their respective intracellular amino acid pool (related to Fig. 1f). Differentiating T_H17 cells or iT_{reg} cells (68 h) were fed with 2 mM [^{15}N]α-glutamine for 4 h. The cells were collected for intracellular metabolites analysis. The ratios of ^{15}N-labelled aspartate, glycine, alanine and serine to their total respective amino acid pools were calculated. **c**, AOA, as a pan-transaminase inhibitor, inhibited *de novo* synthesis for several amino acids (via transamination) in both cell types in addition to aspartate. The ratio of [^{15}N]amino acid to [^{15}N]glutamate was calculated, and this ratio was further normalized to that in T_H17 cells to demonstrate that AOA inhibited *de novo* synthesis for several amino acids. Our rescue results clearly showed (in Fig. 2f, g) that dimethyl-α-KG can largely rescued the effect of AOA on both T_H17 and iT_{reg} cell differentiation. Thus, from a metabolic perspective, the effects of AOA can be largely attributed to its inhibitory effect on α-KG formation (carbon metabolism), rather than its inhibitory effect on amino acid synthesis (nitrogen metabolism). Therefore, we focus on carbon metabolism of glutamate in this study. **d**, GOT1 is the main target for AOA in T_H17 cells. Differentiating T_H17 cells were infected with retrovirus containing shRNA against *Got1* or control shRNA. The GFP$^+$ cells were then purified on day 3, and further cultured under T_H17 cell conditions with/or without AOA. At the end of differentiation (day 6), the cells were collected for analysis of FOXP3 and IL-17 by intracellular staining. It is clear that AOA can further inhibit T_H17 cell differentiation; however, the effect is subtle and supports the conclusion that GOT1 is the main target for AOA under T_H17 conditions. Data in **b** and **c** are mean ± s.d. of three technical replicates from a representative experiment. In **d**, representative flow cytometry data from two experiments are presented.

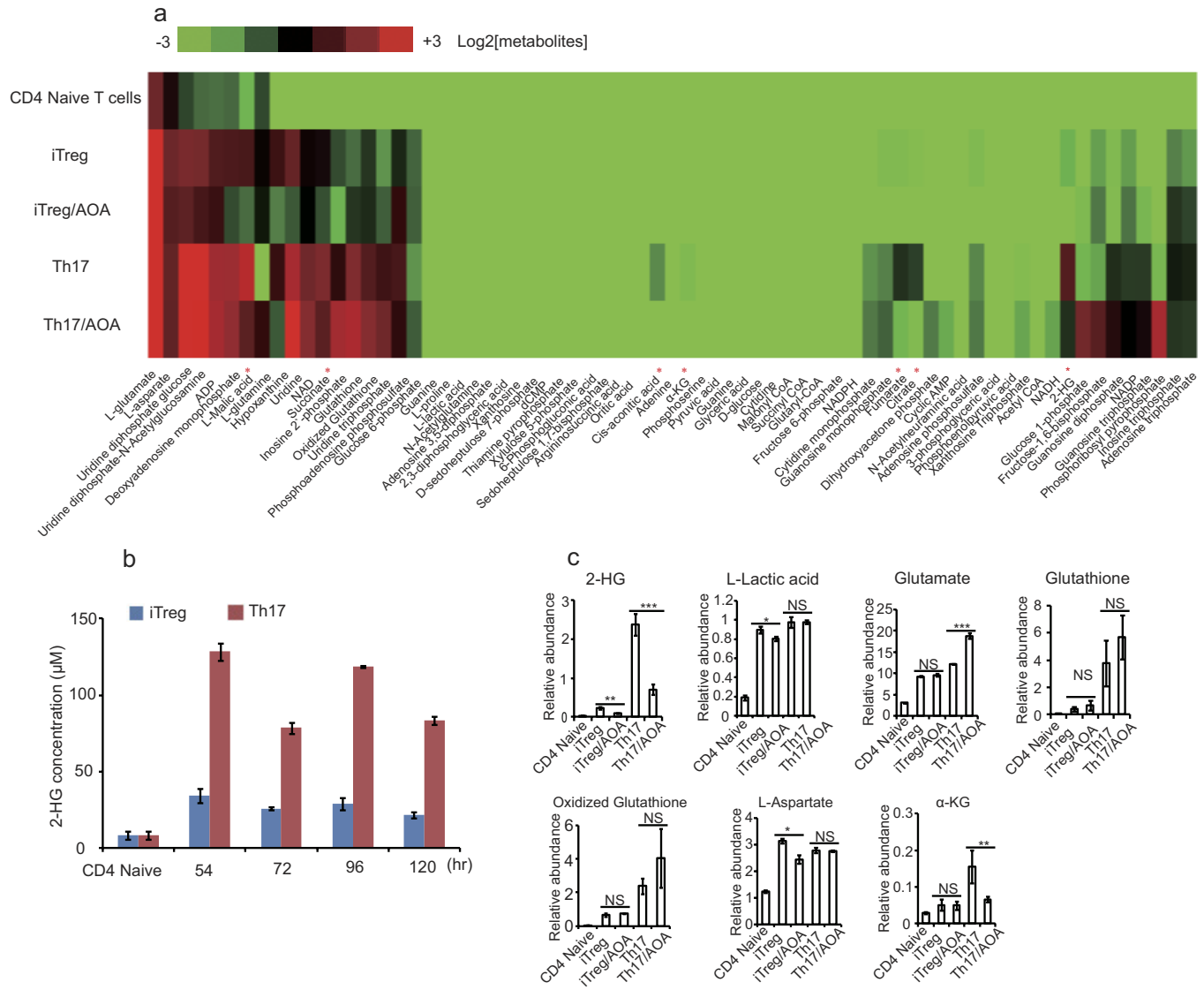

Extended Data Figure 3 | Metabolic profiling of T_H17 cells and iT_{reg} cells. a, Intracellular metabolites profiling of differentiating T_H17 cells and iT_{reg} cells performed by LC–MS. Asterisks denote metabolites with differential abundance between T_H17 and iT_{reg} cells, and this effect is inhibited by AOA. **b**, The 2-HG concentration is much higher in differentiating T_H17 cells than in iT_{reg} cells along the differentiation time line. **c**, AOA significantly decreased the abundance of 2-HG, whereas it did not affect the levels of L-lactic acid, glutathione, oxidized glutathione, L-aspartate, and slightly decreased α-KG and slightly increased glutamate relative to **a**. The relative levels of 2-HG, L-lactic acid, L-glutamate, glutathione, oxidized glutathione, L-aspartate and α-KG from **a** were re-plotted in **c**. Data in **b** and **c** are mean ± s.d. of three replicates from a representative experiment of three independent experiments.

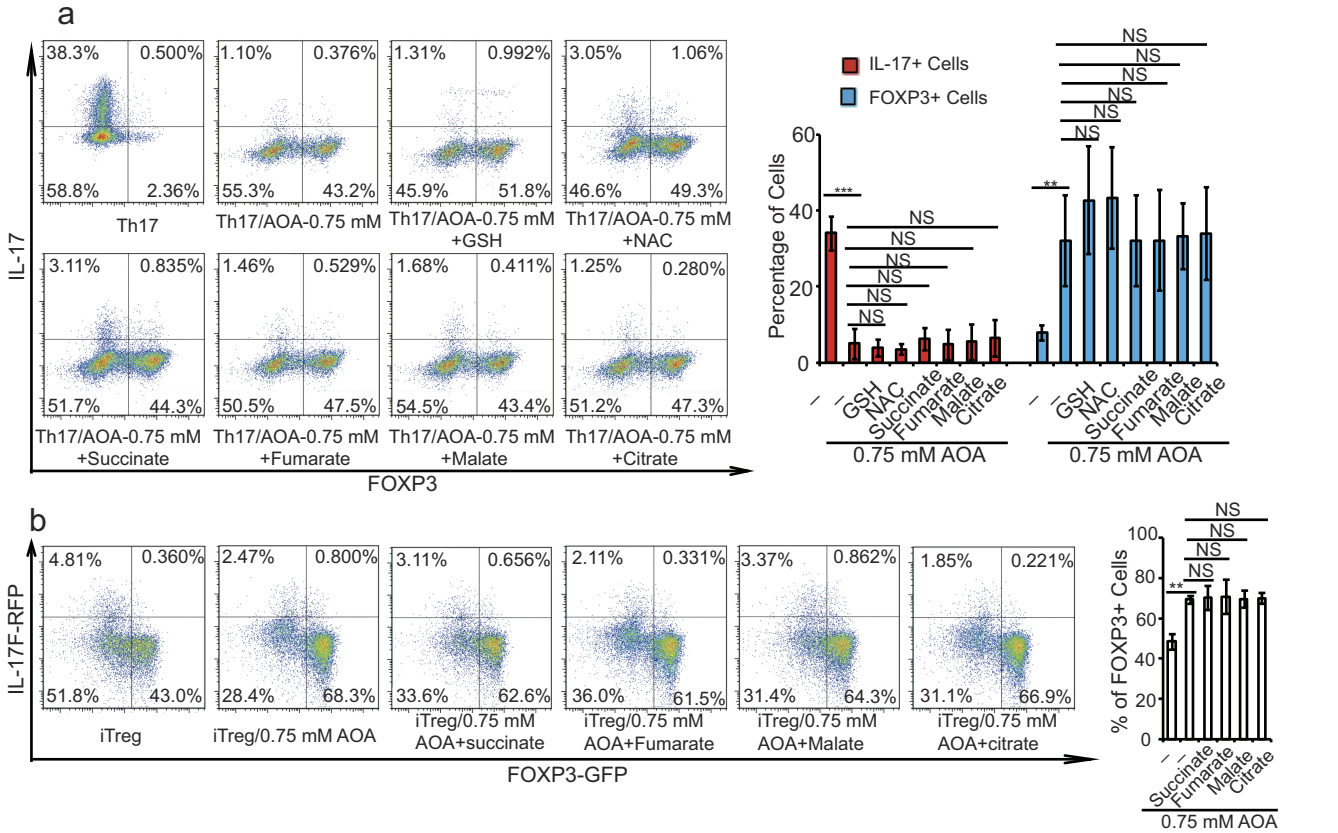

Extended Data Figure 4 | Exogenously added cell-permeable metabolites (citrate, succinate, fumarate and malate) did not rescue the effects of AOA on T_H17 and iT_{reg} cell differentiation. a, Cell-permeable dimethyl esters of succinate, fumarate, malate, citrate, NAC or GSH did not rescue the inhibitory effects of AOA on T_H17 cell differentiation. Cell-permeable metabolites (0.5 mM succinate, 50 μM fumarate, 0.5 mM malate, 0.5 mM citrate, 1 mM NAC, and 1 mM GSH) were individually added to differentiating T_H17 cells in the presence of AOA. At the end of the differentiation (day 6), the cells were re-stimulated and analysed by intracellular staining of FOXP3 and IL-17. **b**, Cell-permeable dimethyl esters of succinate, fumarate, malate or citrate, did not rescue the effects of AOA on iT_{reg} cell differentiation. Cell permeable metabolites (0.5 mM succinate, 50 μM fumarate, 0.5 mM malate, 0.5 mM citrate) were individually added to differentiating iT_{reg} cells in the presence of AOA. At the end of the differentiation (day 5), the cells were directly analysed for FOXP3–GFP. Representative flow cytometry data (left panels) are from three independent experiments. Bar graphs are mean ± s.d. of three independent experiments. $^{**}P < 0.01$; $^{***}P < 0.001$ by Student's *t*-test.

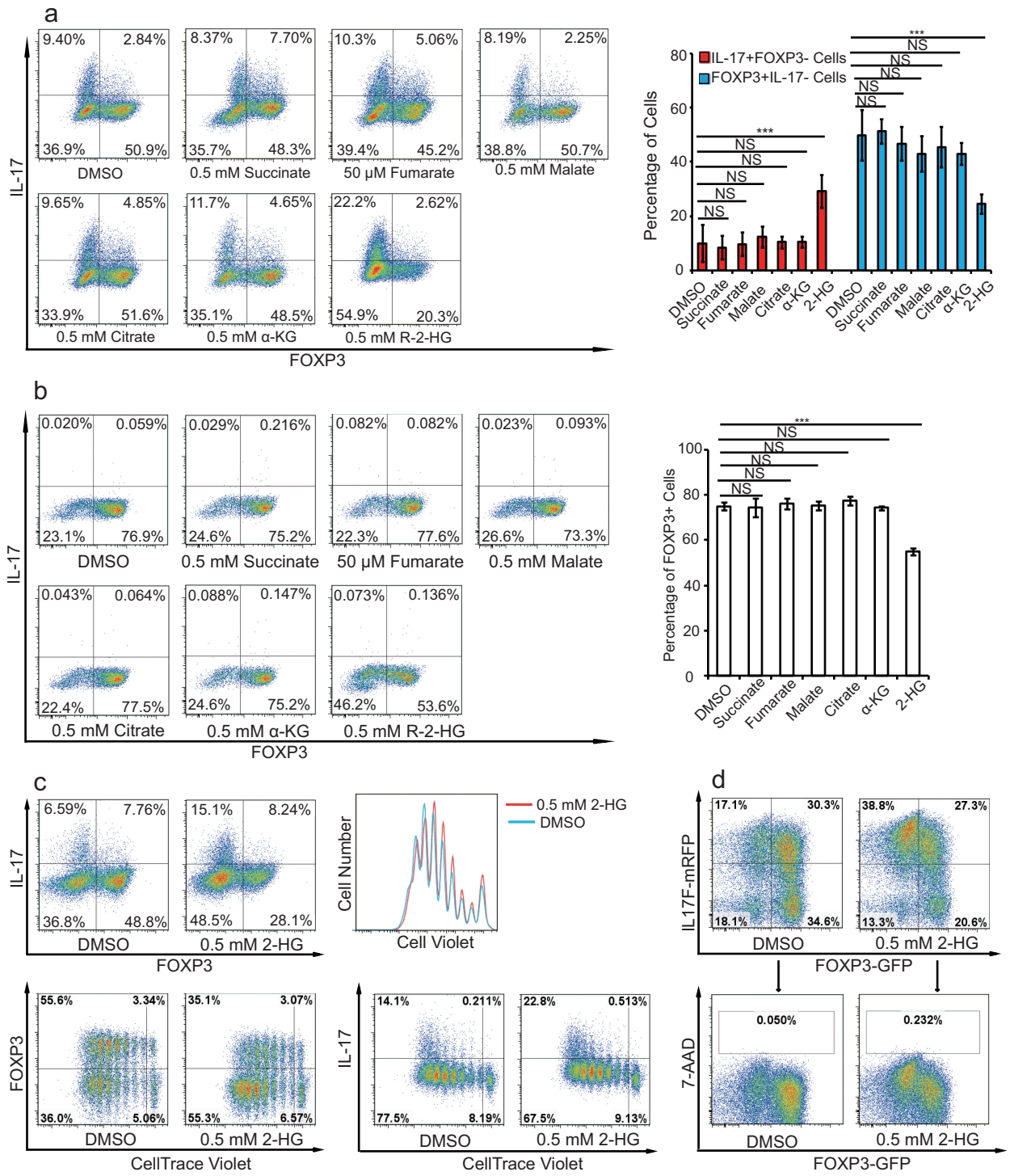

Extended Data Figure 5 | The effect of cell-permeable metabolites (α-KG, 2-HG, citrate, succinate, fumarate and malate) on the differentiation of T_H17 or iT_{reg} cells. a, Indicated dimethyl metabolites were added into T_H17 cell culture, and the cells were analysed on day 4 by intracellular staining of FOXP3 and IL-17. **b**, The indicated metabolites were added to iT_{reg} cell culture, and cells were analysed on day 5 by intracellular staining of FOXP3 and IL-17. **c**, **d**, 2-HG did not affect cell proliferation and survival. **c**, CD4 naive T cells were labelled with CellTrace Violet according to the manufacturer's protocol. The cells were then differentiated under T_H17 cell conditions. The cells were then stimulated and collected for intracellular staining at day 4. **d**, CD4 naive T cells from double-reporter mice were differentiated under T_H17 cell conditions, and live cells were analysed at day 4; 7-AAD was added just before analysis. Representative flow cytometry data are from three independent experiments. Bar graphs are mean ± s.d. of three independent experiments. $***P < 0.001$ by Student's *t*-test.

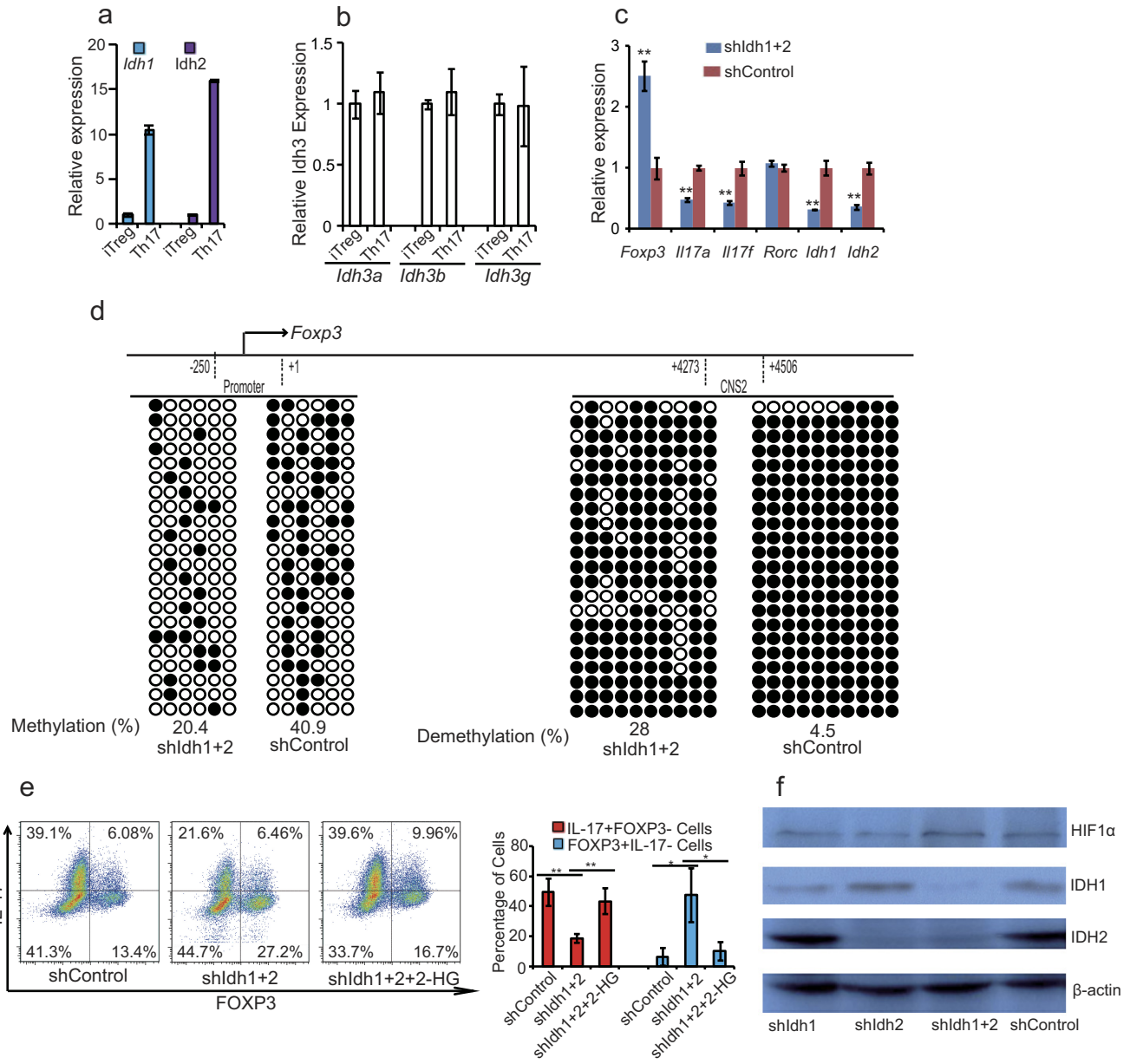

Extended Data Figure 6 | Differentiating T_H17 cells highly express IDH1 and IDH2, and shRNA against IDH1 and IDH2 suppresses the expression of IDH1 and IDH2, decreases DNA methylation at the *Foxp3* locus, and suppresses T_H17 cell differentiation. a, Differentiating T_H17 cells or iT_{reg} cells (day 3) were collected for mRNA expression analysis. All expression levels were normalized to β-actin (*Actb*), and the expression level of each enzyme was normalized to that in differentiating iT_{reg} cells. **b**, Differentiated T_H17 cells and iT_{reg} cells have similar expression levels of IDH3. The experiment was performed as described in **a**. mRNA expression of IDH3 subunits (*Idh3a*, *Idh3b* and *Idh3g*) was normalized to β-actin, and plotted relative to the gene expression level in iT_{reg} cells. **c**, shRNA knockdown of IDH1 and IDH2 efficiently suppressed the mRNA expression of *Idh1*, *Idh2*, *Il17a* and *Il17f*, and increases mRNA expression of *Foxp3*. Infected cells (GFP^+ cells) containing shRNA against IDH1 and IDH2 were FACS sorted and re-stimulated with anti-CD3 and anti-CD28 for mRNA expression analysis. Expression was normalized to β-actin. **d**, shRNA knockdown of IDH1 and IDH2 decreased the methylation level at the *Foxp3* locus. Differentiating T_H17 cells were infected with retrovirus containing *Idh1* and *Idh2* shRNA or control shRNA (shControl). At the end of the differentiation (day 6), GFP^+ cells were collected for DNA methylation analysis of the *Foxp3* promoter and its intronic CpG island by bisulfate sequencing. Filled circles denote methylated cytosine; open circles denote demethylated cytosine. Male mice were used owing to X-chromosome inactivation. **e**, Knockdown of IDH1 and IDH2 suppressed T_H17 cell differentiation, and this can be reversed by addition of cell permeable (*R*)-2-HG. Cell permeable (*R*)-2-HG was added to differentiating T_H17 cells at 6 h. The cells were infected with retrovirus containing shRNA. GFP^+ cells were purified at day 3 for further culture under T_H17 cell conditions, and cell permeable (*R*)-2-HG was added to the culture until the end of the experiment. Cells were then collected for analysis of FOXP3 and IL-17. **f**, Knockdown of IDH1 and IDH2 has minimal effect on HIF1α expression. Differentiating T_H17 cells were infected with retrovirus containing *Idh1* shRNA, *Idh2* shRNA and *Idh1* plus *Idh2* shRNA or control shRNA. Cells were then analysed for IDH1, IDH2 and HIF1α expression. Data in **a**–**c** are mean ± s.d.($n = 3$) of three technical replicates from a representative experiments of three experiments. Data in **e** ($n = 3$) are mean ± s.d. of three independent experiments. $*P < 0.05$; $**P < 0.01$; $***P < 0.001$ by Student's *t*-test.

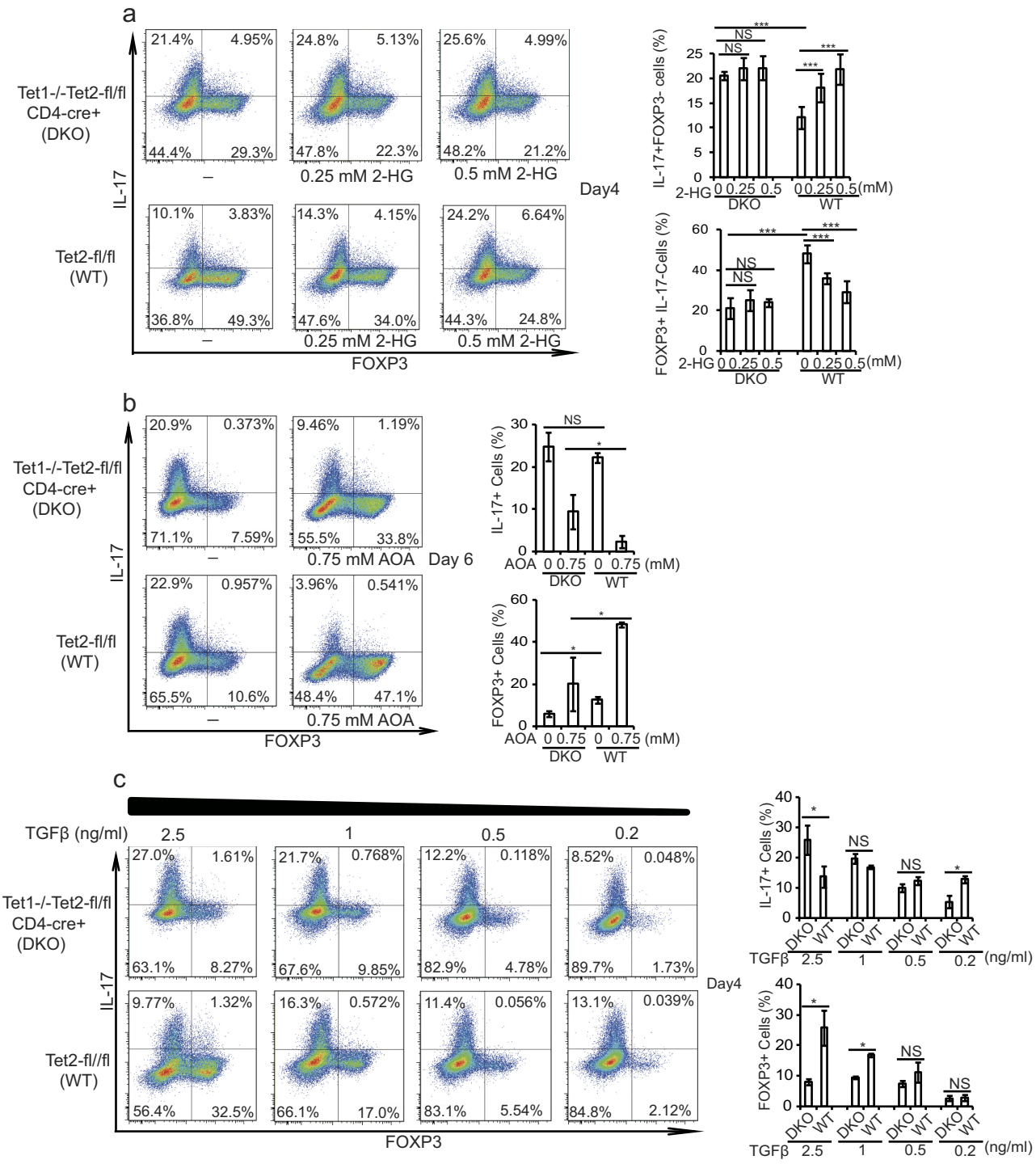

Extended Data Figure 7 | See next page for caption.

Extended Data Figure 7 | TET1 and TET2 control FOXP3 expression during T_H17 cell differentiation. a, *Tet1* and *Tet2* double-knockout (DKO; *Tet1*$^{-/-}$*Tet2*$^{fl/fl}$CD4-Cre^{+}) promoted T_H17 cell differentiation, and largely abrogated the promoting effect of (*R*)-2-HG on T_H17 cell differentiation in wild-type T cells. CD4 naive T cells from *Tet1/2* DKO or control mice were differentiated under T_H17 cell conditions with or without cell permeable (*R*)-2-HG. At day 4, cells were collected for analysis of FOXP3 and IL-17 by intracellular staining. Results are consistent with a previous study that showed that *Tet1/2* DKO regulatory T cells can be more easily and efficiently converted into T_H17 cells[15]. **b**, *Tet1/2* DKO partially diminished the inhibitory effect of AOA on T_H17 cell differentiation. CD4 naive T cells from *Tet1/2* DKO or control mice were differentiated under T_H17 cell conditions with or without AOA. Cells were collected for analysis of FOXP3 and IL-17 at day 6. **c**, A reduced concentration of TGFβ largely abolished the effect of *Tet1/2* DKO on T_H17 cell differentiation, and *Tet1/2* DKO decreased IL-17 expression when the TGFβ concentration is low enough, indicating that TET1/2 proteins have a dual function in the fate determination of T_H17 cell differentiation. CD4 naive T cells derived from *Tet1/2* DKO or control mice were differentiated under T_H17 cell conditions with varied concentrations of TGFβ. Cells were collected for intracellular analysis at day 4. A previous study showed that TET2 positively regulate T_H17 differentiation by binding to the *Il17a* gene locus[23]. However, our results show that *Tet1/2* DKO T cells enhance T_H17 cell differentiation, as determined by increased IL-17 and reduced FOXP3 expression at day 4 in T_H17 cell culture. Because Tet enzyme activity is very sensitive to various exogenous stimuli, as described previously[16], the discrepancy between our results and those of Ichiyama *et al.*[23] could be caused by different culture conditions, in which our T_H17 polarizing condition yielded a high amount of FOXP3 even at later stage of T_H17 differentiation (day 4). To test this, we reduced the amount of TGFβ in our cultures, and consistent with Ichiyama *et al.*[23], *Tet1/2* DKO caused a significant reduction in T_H17 cell differentiation under low TGFβ concentrations (**c**). A high TGFβ concentration may induce strong and persistent activation of SMAD3 and STAT5, which then recruit TET enzymes to the *Foxp3* gene locus and promote its expression by inducing or maintaining the demethylation status[15]. Conversely, a low TGFβ concentration results in recruitment of TET enzymes to the *Il17* gene locus, which plays a dominant role in regulating T_H17 differentiation. We have thus identified dual functions of TET proteins in the fate determination of T_H17 cell differentiation. In summary, the role of TET1/2 during T_H17 cell differentiation is dynamic and dependent on the expression of FOXP3. In **a**–**c**, representative flow cytometry data from five (**a**), three (**b**) and two (**c**) independent experiments are shown. In **a** and **b**, bar graphs are mean ± s.d. of five (**a**) or three (**b**) independent experiments. In **c**, bar graphs are mean ± s.d. of three technical replicates from a representative experiment of two independent experiments. $^{*}P < 0.05$; $^{***}P < 0.001$ by Student's *t*-test.

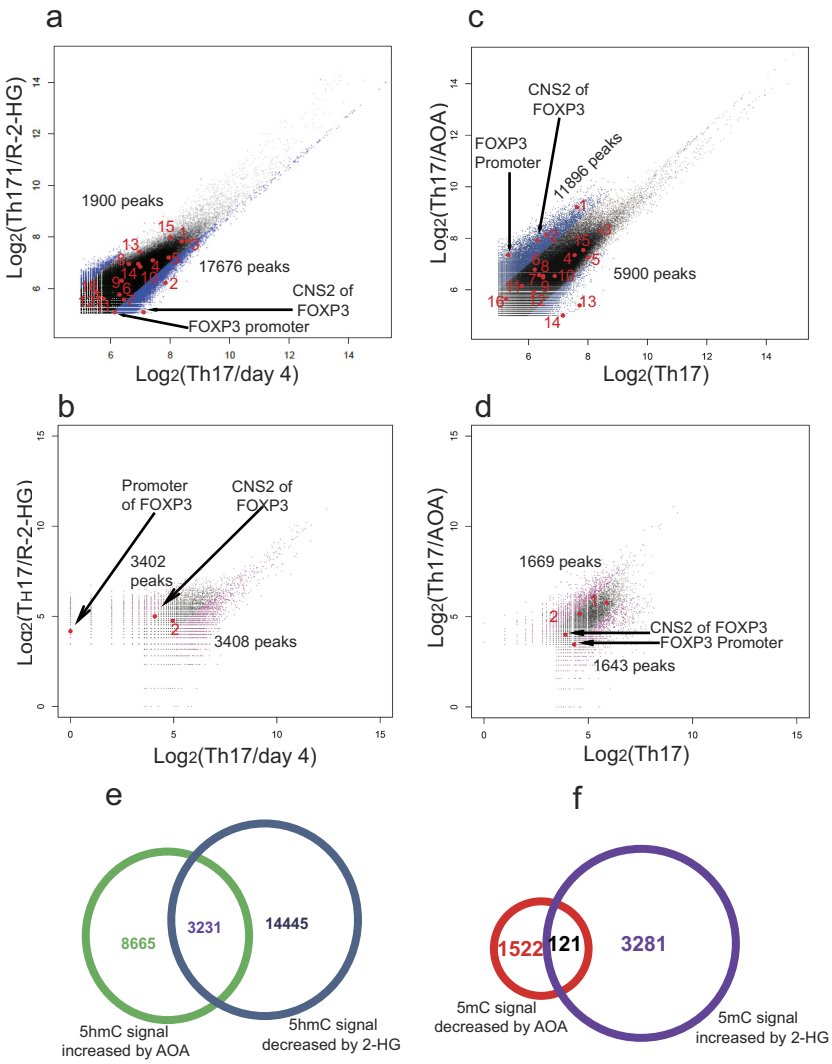

Extended Data Figure 8 | AOA and (*R*)-2-HG selectively affect DNA hydroxymethylation and methylation at the *Foxp3* locus, but not other important lineage-specific signature gene loci examined by (h)MeDIP–seq. a, **b**, Exogenous addition of dimethyl-(*R*)-2-HG selectively decreases the 5hmC signal and increases the 5mC signal at the *Foxp3* locus. DNA extracted from differentiating T_H17 cells (day 4) in the absence or presence of 0.75 mM dimethyl-(*R*)-2-HG was immunoprecipitated with antibodies to 5hmC (**a**) or 5mC (**b**), followed by deep sequencing (see Methods). **a**, Differential peaks from hMeDIP. 5hmC peaks located in the *Foxp3* conservative region or in other conservative regions such as *Il4*, *Il5*, *Il13*, *Il10*, *Ifng* and *Rorc* were highlighted. Peaks 1, 2 and 11 were located in *Gata3*; peak 3 in *Rorc*; peak 4 in *Il4*; peaks 5 and 16 in *Il10*; peak 6 in *Ifng*; peaks 7 and 10 in *Il5*; peaks 8 and 9 in *Tbx21*; peaks 12 in *Il13*; peaks 13 and 15 in *Il17a*; peak 14 in *Il17f*. (*R*)-2-HG decreased the 5hmC signal in 17,676 out of 330,582 peaks detected. However, (*R*)-2-HG did not decrease DNA hydroxymethylation at *Il4*, *Il5*, *Il10*, *Il13*, *Il17a*/f, *Ifng*, *Rorc* and *Tbx21* loci. **b**, The 5mC signal was increased in 3,402 out of the 17,676 peaks with a decreased 5hmC signal. (*R*)-2-HG selectively decreased the 5hmC signal and increased the 5mC signal at the *Foxp3* promoter and CNS2 region, but did not affect the 5hmC or 5mC signal at *Ifng*, *Il4/5/10/13*, *Il17a/f*, *Tbx21* or *Rorc*. Notably, exogenous dimethyl-(*R*)-2-HG did not affect the 5hmC or 5mC signal at only the *Foxp3* locus, and instead had a more broad effect at many loci. **c**, **d**, AOA treatment selectively affect DNA hydroxymethylation and methylation at the *Foxp3* locus. 5hmC peaks located in the *Foxp3* conservative region or in other conservative regions such as at *Il4*, *Il5*, *Il13*, *Il10*, *Ifng* and *Rorc* were highlighted; labels are as in **a**. AOA increased the 5hmC signal in 11,896 out of 330,582 peaks detected. AOA increased hydroxymethylation at the *Foxp3* promoter and CNS2 region, but did not affect DNA hydroxymethylation at regions such as *Ifng*, *Il4*, *Il5*, *Il10*, *Il13*, *Rorc* and *Tbx21*. Notably, AOA treatment reduced the 5hmC signal at *Il17a/f* loci, probably owing to the antagonistic effect of FOXP3 on RORγt to recruit TET proteins to *Il17a/f* loci. **d**, The 5mC signal was increased in 1,643 out of the 11,896 peaks with an increased 5hmC signal. AOA decreased the 5mC signal at the *Foxp3* promoter. Notably, changes in the 5mC signal at the *Foxp3* CNS2 region were not detected, probably because the CNS2 region is largely methylated (around 70–80% of it is methylated in iT_{reg} cells), and changes in 5mC are more subtle and harder to detect than changes in 5hmC. Notably, both AOA and 2-HG affected the 5hmC, but not 5mC, signal at *Gata3*. However, *Gata3* expression is not regulated by DNA hydroxymethylation as shown in a previous study[23], therefore 2-HG and AOA are unlikely to affect *Gata3* expression. **e**, 17,676 peaks with increased 5hmC signal by AOA (from **a**, blue) overlapped with 11,896 peaks with decreased 5hmC signal by 2-HG (from **c**, green). **f**, 3,402 peaks with increased 5mC by 2-HG (from **b**, purple) overlapped with 1,643 peaks with decreased 5mC signal by AOA (from **d**, red). These epigenetic analyses showed that the effect of AOA and 2-HG on *Foxp3* compared with other T-lineage-related genes is highly selective, despite their more broad effects on genome-wide DNA methylation and hydroxymethylation. Although demethylation at the *Foxp3* locus promotes FOXP3 expression, the expression of many other genes is not regulated by DNA demethylation, such as *Rorc* and *Gata3*[23]. Treatment of T cells with AOA under T_H17 cell conditions stabilizes FOXP3 expression, but does not have much of an effect on the expression of other lineage-specific transcription factors, such as *Gata3* and *Rorc*. FOXP3 can antagonize the function of RORγt to suppress expression of T_H17 cell signature genes as well as recruit DNMT1 to the gene loci of proinflammatory cytokines or signature genes to promote methylation at these loci, suppressing their expression[24]. In addition, FOXP3 functions as both a transcriptional activator to directly activate its target genes required for iT_{reg} cell differentiation/function, and a transcriptional repressor to directly suppress the genes associated with effector T cell function, resulting in iT_{reg} cell fate[25].

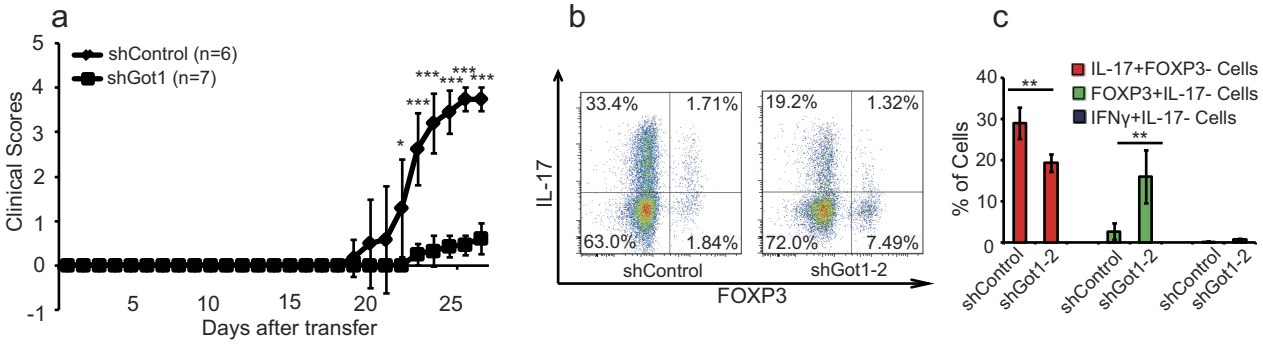

d. Quantification of cell numbers infiltrated into CNS

		Mononuclear Cells (Mean± s.e.m.)	IL-17+FOXP3- Cells (Mean± s.e.m.)	FOXP3+IL-17- Cells (Mean± s.e.m.)	FOXP3+ Cells/IL-17+Cells
Related to Fig.4a-c	PBS	791,143±100,439	72,763±9,633	69,131±9,510	0.950
	AOA	325,000±78,179	15,423±3,945	26,983±8,144	1.750
Related to Fig.4d-g (Retrieved from FACS)	shControl	50,000±0	6,461±933	1,080±117	0.167
	shGot1-1	19,804±5,555	575±420	657±326	1.143
Related to Extended Data Fig.9 (a-c)	shControl	618,333±77,949	62,171±16,143	4,592±783	0.074
	shGot1-2	130,714±27,177	7,594±1,452	5,924±1,146	0.78

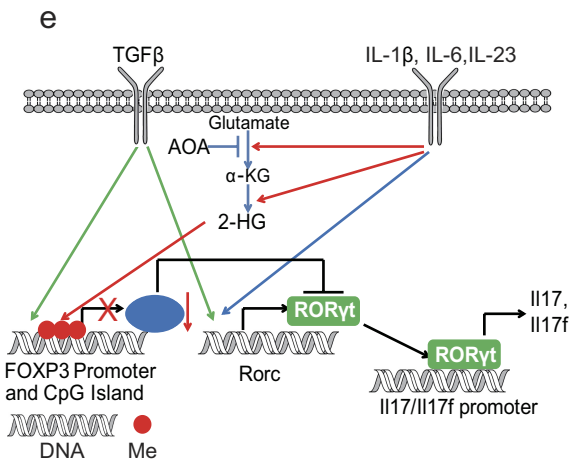

Extended Data Figure 9 | shRNA knockdown of GOT1 ameliorated mouse EAE in a T_H17-polarized adoptive transfer EAE model. **a**, Disease score. **b**, The T cells infiltrated into the central nervous system were analysed (gated on Thy1.1$^+$ cells), and representative flow cytometry data are shown. **c**, Statistics for the T cells infiltrated into the central nervous system (CNS). Data in **a** and **c** are mean ± s.d. $^*P < 0.05$; $^{**}P < 0.01$; $^{***}P < 0.001$ by Student's *t*-test. **d**, Quantification of the numbers of cells infiltrated into the central nervous system regions. **e**, Schematic of our mechanistic model. The cell number in Fig. 4d–g was retrieved from flow cytometry data. Although we did not count the number of individual populations, we noticed that the total number of cells infiltrating into the central nervous system was reduced by *Got1* shRNA; fewer than 50,000 cells were recovered from the *Got1* shRNA group, whereas more than 50,000 cells were recovered from control mice. Thus, for mice receiving T cells infected with shRNA control virus, the cell number was calculated from a total of 50,000 live cells acquired by flow cytometry (this group of mice had a much higher number of total infiltrated cells, and we stopped acquiring cells after the total number reached the 50,000 threshold). Mice receiving T cells infected with *Got1* shRNA virus had fewer cells infiltrated into the central nervous system, and collected cells did not reach the 50,000 threshold during flow cytometry; therefore, the cell numbers represent all of the cells infiltrated into the central nervous system. Despite the low accuracy, *Got1* shRNA decreased the total absolute number of cells infiltrated into the central nervous system. For two other EAE experiments, cell numbers were counted immediately after isolating cells from the central nervous system.